STRUCTURE IN LIQUID TRIGLYCERIDES

by

Liangle Lin

Submitted in partial fulfilment of the requirements
for the degree of Master of Science

at

Dalhousie University
Halifax, Nova Scotia
October 2014

TABLE OF CONTENTS

LIST OF TABLES

LIST OF FIGURES

ABSTRACT

The structure and distribution of triglycerides (TAGs) in fats affects the properties of the final products, in terms of texture, appearance and mouth feel. A few debates and models have been developed on the distribution of TAG molecules in the liquid, but they are not consistent with the actual density of oils or our X-ray scattering (XRS) data.

Four pure liquid TAG samples were examined by XRS at temperatures up to 210 °C. WAXS data are consistent with the liquid phase of alkanes and other aliphatic molecules. SAXS data are similar to those produced by alcohols and fatty acids, whose molecules associate via polar groups. Therefore, we developed a new conceptual model to describe the clustering of liquid TAGs as "Loose Multimers" and from it estimated that they consist approximately of 5 to 9 molecules. The average number of molecules decreases with temperature and increases with molecular weight.

LIST OF ABBREVIATIONS AND SYMBOLS USED

CCD	charged-couple device
ccp	cubic close packing
cn	carbon number
d_{c-c}	distance between center of molecules
f_m	atomic scattering densities
FWHM	full width at half maximun
G	Gibbs energy (J)
H	enthalpy (J)
hcp	hexagonal close packing arrangement
LLL	trilaurin
LM	Loose Multimer
M_W	molecular weight (g/mol)
M_{sm}	mass of a single molecule (g)
n	an integer representing the order of the diffraction peak
N_A	Avogadro number
N_{LM}	number of molecules in each Loose Multimer
NMR	nuclear magnetic resonance
NSLS	National Synchrotron Light Source
PPP	tripalmitin
r_{c-c}	average characteristic distance between centers (nm)
rhdh	rhombic dodecahedra
r_{LM}	radius of a Loose Multimer

rzk, rtk, rck	coefficients used to determine the density of TAG molecules
S	entropy (J/K)
SAXS	small-angle X-ray scattering
SSS	tristearin
T	temperature (˚C)
TAG	triglyceride or triacylglycerol
T_m	melting temperature (˚C)
V	volume of the molecule (nm^3)
V_{LM}	volume of each Loose Multimer (nm^3)
V_{sm}	volume occupied by a single molecule (nm^3)
WAXS	wide-angle X-ray scattering
XRD	X-ray diffraction
XRS	X-ray scattering
$\boldsymbol{\lambda}$	wavelength of the X-ray beam (Å)
$\boldsymbol{\theta}$	the Bragg angle (˚)
$\boldsymbol{\rho}$	density ($g/cm^{3)}$
$\boldsymbol{\rho_{(r)}}$	electron density per unit volume at a distance r from the reference atom
$\boldsymbol{\rho_0}$	average electron density in the sample
$\boldsymbol{\delta q}$	full width at half maximum of the scattered peak ($Å^{-1}$)

ACKNOWLEGEMENTS

I would first like to thank my supervisor, Dr. Gianfranco Mazzanti, for his support, patience, encouragement, helpfulness and willingness to teach. I have learned a lot during my time here and I consider it to have been a very great opportunity for me to come to Halifax and do research with the Mazzanti group. I am indebted to the deep insights of Dr. David Pink, and the feedback from Dr. Jan Haelssig. The use of the Nanostar instrument was kindly granted by Dr. Jeff Dahn, with the technical support from Dr. Robbie Sanderson. Technical assistance at the synchrotron was provided by Steve Bennett.

I would also like to thank all my research colleagues: Omar Al-Qatami, Pavan Karthik Batchu, Amro Alkhudair, Rong Liu, Mohit Kalaria, Pranav Arora, Xiyan Deng and Yujing Wang. Thanks for making this time a very pleasant one.

Finally, I'd like to express gratitude to my family and friends, whose encouragement and support has helped me all the way.

CHAPTER 1 INTRODUCTION

Fats or lipids, mainly made of triglycerides (TAGs), are the key ingredients in many very popular foods, like ice cream, chocolate, margarine, etc. The structure and distribution of TAGs affects the properties of the final products, in terms of texture, appearance and mouth feel (Himawan, Starov & Stapley, 2006; Metin & Hartel, 2005).

A few models have been proposed to describe the distribution of TAGs molecules in their liquid state. Larsson (1972) proposed a popular lamellar model, but it turned out to be inconsistent with the small angle neutron scattering data from Cebula et al. (1992). On the other hand, molecular modeling by Sum et al. (2003) supported the lamellar hypothesis. The recent discotic model proposal by Corkery et al. (2007) is not consistent with the actual density of oils or with our observations of SAXS from liquid TAGs X-ray scattering (XRS) data obtained as collateral data prior to hundreds of time-resolved crystallization experiments. Limited molecular association was predicted by simulation studies on liquid alkanes (Fujiwara & Sato, 1999; Takeuchi, 1998). Some degree of transient clustering was also observed, though not quantified, in simulations on TAGs conducted by Hall, Repakova, & Vattulainen (2008); Hsu & Violi (2009) and Pink et al. (2010)

X-rays have been used for a very long time in studying TAGs crystalline phases. X-ray diffraction (XRD) and XRS are fundamentally similar because both methods use intense beams of X-ray to obtain structural information of the sample. Differences arise from making measurements of target molecules in solutions or liquid state (XRS) or embedded in a crystal (diffraction). Both are forms of elastic scattering that provide

information on spatial distribution of electron densities. TAGs produce two regions of XRS patterns: small-angle (SAXS) and wide-angle (WAXS). WAXS comes from the short distance between the aliphatic chains, and is essentially similar to that of alkanes. SAXS probably arise from the long distance between the glycerol cores, since the differences in electron density between cores and chains produce scattering

As derived by Debye (1947), the scattering intensity is the product of the scattering amplitude by a noncrystalline array of atoms at a given reciprocal scattering vector "q" as a function of scattering angles (Klug & Alexander, 1974). Since Bragg's law cannot apply strictly to XRS in liquid, Klug & Alexander (1974) introduced the "R-spacing" and described its relationship to Bragg's "d". These concepts will be used in this Thesis to interpret the scattering data.

This research aims to find out how TAGs molecules are distributed in the liquid and develop a model to better describe their distribution, based on our XRS observations and modeling or experimental literature reports.

Our hypothesis is that, in their liquid melt, TAGs molecules associate to form clusters, that have on average 5 to 9 molecules.

Four pure TAG samples were used: trilaurin (LLL), trimyristin (MMM), tripalmitin (PPP) and tristearin (SSS). A series of XRS experiments were performed on the X10A beamline (wavelength 1.0889 Å) in the National Synchrotron Light Source at Brookhaven National Laboratory, and in the Dunn building of the Physics Department at Dalhousie University (wavelength 1.541 Å). Each sample was kept in a capillary at high temperature while SAXS and WAXS data were being collected.

CHAPTER 2 LITERATURE REVIEW

2.1. Triglycerides

Fats and lipids are widely used in food, cosmetics, pharmaceuticals, etc. (Gunstone & Padley, 1997). They are heavily present in commercial fat products, such as chocolate, margarine, butter, and baked goods. Both processing and storage conditions are important determinants in food quality, texture, and shelf-life (Himawan, Starov & Stapley, 2006; Metin & Hartel, 2005). TAGs are the main component of edible fats constituting from 95% to 98% of the composition (Metin & Hartel, 2005). They are composed of three fatty acids units (R_1, R_2, R_3) attached to one glycerol unit. The typical structure of TAG molecules is shown in Figure 2-1 (a) (Sato, 2001). In our research, four simple TAGs were used, which contain only one type of fatty acid (as shown in Table 2-1) (Sato et al., 1999).

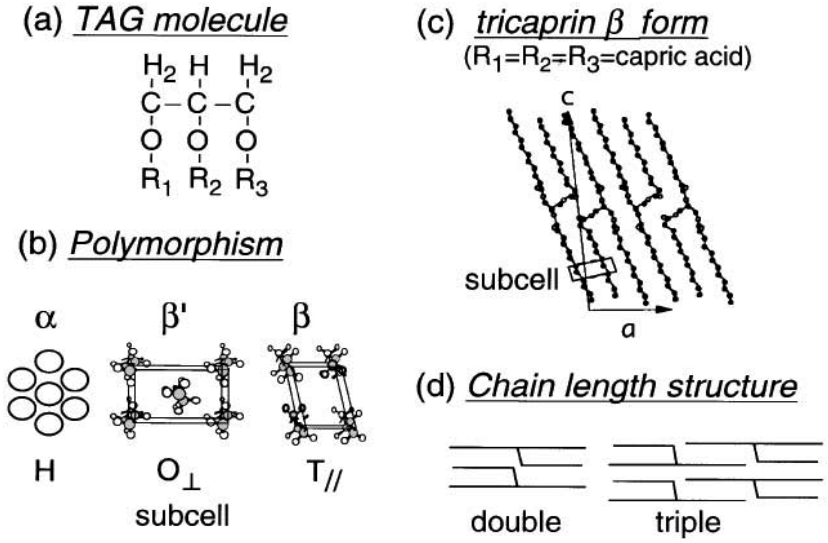

Figure 2-1(a) A general TAG molecule structure, (b) the subcell structures of three most common polymorphisms in TAGs, (c) unit cell structure of tricaprin ß form and (d) chain length structure in TAGs (Sato, 2001).

Table 2-1 Fatty acids in TAG samples used in our research.

Code	Fatty acid	Chain Length
L	lauric acid (dodecanoic acid)	12
M	myristic acid (tetradecanoic acid)	14
P	palmitic acid (hexadecanoic acid)	16
S	stearic acid (octadecanoic acid)	18

2.1.1. Polymorphism

The polymorphic crystalline structure of fats was studied long before any interest arose in their liquid state, and seems to have influenced the initial ideas of possible structure in the liquid. Polymorphism is the ability of a molecule to form more than one crystalline structure depending on its arrangement within the crystal lattice (Metin and Hartel, 2005). The crystallization behavior of the TAGs are directly influenced by polymorphism, which is influenced by molecular structure itself, and by several external factors such as temperature, pressure, solvent, rate of crystallization, impurities (Sato, 2001). TAG molecules packed in different crystalline arrangements exhibit significantly different melting temperature, shown in Table 2-2 (M. Takeuchi, Ueno, & Sato, 2003).

Table 2-2 Melting point (˚C) of the three polymorphic forms for LLL, MMM, PPP, SSS (M. Takeuchi et al., 2003).

	α	β	β'
LLL	15	35	46.5
MMM	33	46.5	57
PPP	44.7	56.6	66.4
SSS	54.9	64	73.1

There are three common polymorphs of fats: α, β and β' (Larsson, 1966). The differences between polymorphs come from their subcell structure and are apparent from a top view of these planes, as seen in Figure 2-1 (b). α is an unstable form in which the

hydrocarbon chains are packed in a hexagonal (H) type subcell. β' is a metastable form that has an orthorhombic perpendicular ($O_\perp$) subcell. β is the most stable form and has a triclinic parallel ($T_{//}$) subcell (Takeuchi et al., 2003). Subcell structures are defined as cross-sectional packaging of the zigzag aliphatic chains (Sato, 2001). The chain length structure produces a repetitive sequence of the acyl chains involved in a unit cell lamella along the long-chain axis. The stacking of these chains can be in either a double or triple chain length structure, shown in Figure 2-1 (d). A double chain length structure usually occurs when the chemical properties of the three acid moieties are the same or very similar, as shown in Figure 2-1 (c) of tricaprin β form (Jensen & Mabis, 1966).

The Gibbs energy (G) determines the thermodynamic stability of the polymorphic forms of TAGs; the polymorph that has the lowest G is the most stable. G-Temperature (T) diagram is shown in Figure 2-2 for the three basic polymorphs of TAGs. The plot follows the equation for G as a function of enthalpy (H), entropy (S) and T, which is:

$$\Delta G = \Delta H - T\Delta S \quad (1)$$

The ΔG values are the largest for the α form, intermediate for the β' form and smallest for the β form. Each polymorphic form has its own melting temperature, T_m, shown as the intersection points of the G-T curves of the polymorphs and the liquid phase.

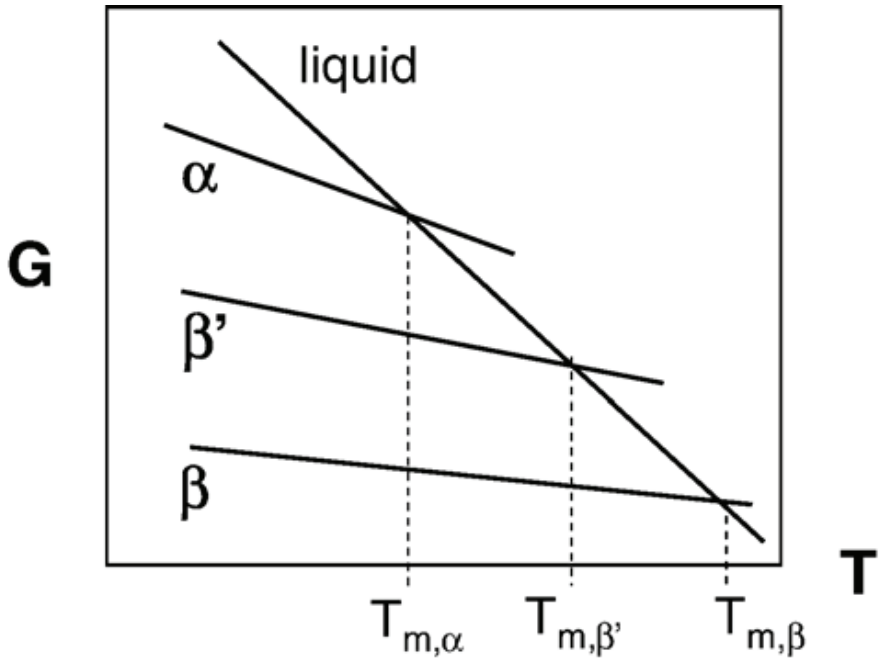

Figure 2-2 The relation between Gibbs energy and temperature for the three main polymorphic forms of TAGs (Himawan et al., 2006).

2.1.2. Liquid Structure of TAGs

Initial attempts to ascribe a liquid structure to the TAG melts seem to have stemmed from an extension of the polymorphic concept towards the next level of disorder, e.g. at energy contents above the α polymorph. Thus, it has been proposed that a liquid crystalline phase exists in some fat systems before the crystallization of TAGs, unless the temperature is far enough above the melting point to totally destroy this ordering (Hernqvist, 1984; Larsson, 1972; Ueno et al., 1997). Below the melting point, the molecules in the liquid phase would spontaneously organize themselves into these liquid crystals, prior to the formation of actual crystals. This hypothetical liquid crystal structure may also explain the "crystal memory", a phenomenon where fat tends to form the same

crystal structure before melting as the ordering of the liquid phase at the beginning of crystallization (Hernqvist, 1984).

Figure 2-3 a (left) proposed structure of TAGs in liquid by Larsson (1972); b (middle) proposed structure of TAGs in liquid by Cebula et al., (1992); c (right) proposed "Y"-conformation within each "disc", where TAG fatty acid chains spread out at ~120˚ to each other in a single, though diffuse, plane (Corkery et al., 2007).

Since Larsson first proposed the lamellar model based on XRD measurements, as seen in Figure 2-3 (a), a few debates and models were brought up. By incorporating Raman spectroscopy into the methods, Hernqvist (1984) showed that the order of TAGs melt was quite constant and the order of different segments in the hydrocarbon chains varied with different chain length. This smectic structure was also supported by Callaghan & Jolley (1977) through ^{13}C Nuclear Magnetic Reasonance (NMR) measurements. However, Cebula, et al. (1992) claimed that a nematic phase of liquid crystals was more consistent with their observation from SANS experiments, shown in Figure 2-3 (b), instead of the organized molecular aggregates of the smectic liquid crystals in Larsson's model. On the other hand, molecular modeling by Sum et al. (2003) supported the lamellar hypothesis. More recently, an alternative discotic model has been proposed by Corkery, et al. (2007) that triglyceride molecules exist in the liquid state with fully splayed chains ("Y" shape), forming discs structure, shown in Figure 2-3 (c).

These discs then stacked into flexible short cylindrical rods-packing order. However, the discotic model is not consistent with the actual density of oils or with our vast database of liquid TAGs XRS data. Molecular dynamics simulations done by Hsu & Violi (2009) and Hall, Repakova, & Vattulainen (2008) do not support Sum's (2003) proposal of layered structure in liquid TAGs. Hall (2008) pointed out that the liquid system is different from the crystalline-like system and shows a random conformation. In addition, Hsu (2009) reported that liquid TAG molecules with longer aliphatic chains present a higher degree of recoil and hence a greater entanglement between molecules. With Raman Spectroscopy measurements and computer simulations of LLL in the liquid phase, Pink et al. (2010) studied the transition between h-Y conformations, and denied the lamellar model (Larsson, 1972), the discotic packing (Corkery et al., 2007) and the nematic model (Cebula et al., 1992). The idea of a "soft" solid-liquid transition was supported by Da Silva & Rousseau (2008) by studying the ß polymorph to liquid phase transition of five monosaturated TAGs using Raman spectroscopy. Besides, Pink et al. (2010) found in the simulations that the liquid phase exhibits the formation of clusters due to nonzero attractive dipole-dipole interactions via the C=O group, which they thought may give rise to the observed peak in the scattering function at d ≈ 4.6 Å in the WAXS region. The scattering at that "d" value, however, is also largely produced by the alkyl chains, and is therefore not a proof of proximity between glycerol cores of different molecules. This WAXS prediction is in agreement with the work of Stewart & Morrow (1927) on alcohols and Ovchinnikov et al. (1976) on unbranched alkanes. However, numbers of molecules in each cluster was not looked into either in simulations or experimentally in previous studies.

In order to understand what is the distribution of TAGs in their liquid state, apart from the glycerol cores, it is important to understand the distribution of the aliphatic chains. De Gennes (1971) discussed possible motion for one polymer molecule performing wormlike displacements in a strongly cross-linked polymer gel (reptation) and first predicted that the overall mobility and diffusion coefficients of the primitive chain depend strongly on molecular weight. With the help of De Gennes's results, Doi & Edwards (1978a, 1978b, 1979) studied the dynamics of polymers in melts and presented a mathematical model to describe the Brownian motion of polymers. The chains are entangled and cannot pass through each other, which confines each chain inside a tube-like region (figure 2-4), along which it displaces itself. The center line of such a tube-like region was called the primitive path, and can be regarded as the shortest curve which has the same topology as the real chain relative to the other polymer molecules. The primitive chain was characterized by the step length and a diffusion coefficient. The motion inside the tube is thus some kind of reptation. The step length of the primitive chain may be thought as a mean intermolecular distance.(Doi & Edwards, 1978b; Doi, 1975).

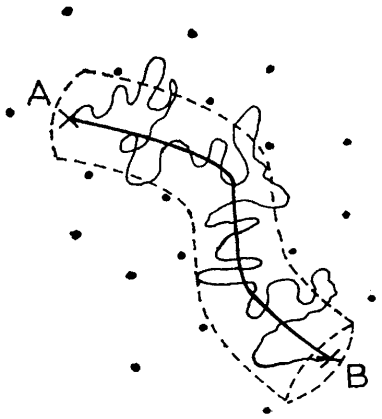

Figure 2-4 Chain segment AB in dense rubber. The points A and B denote the cross-linked points, and the dots represent other chains which, in this drawing, are assumed to be perpendicular to the paper. Due to entanglements the chain is confined to the tube-like region denoted by the broken line. The bold line shows the primitive path (Doi & Edwards, 1978b).

Many experiments and modeling have been done on liquid alcohols (Chapman et al., 1990; Franks et al., 1993; Stewart & Morrow, 1927; Stewart, 1927), alkanes (Christenson et al., 1987; Goodsaid-Zalduondo & Engelman, 1981; Ovchinnikov et al., 1976; Venturi et al., 2009), fatty acids (Iwahashi et al., 2004) and paraffins (Stewart, 1927, 1928). Iwahashi (2004) found that fatty acids exist mostly as dimers and the dimers aggregate to form clusters possessing a "quasi-smectic" liquid crystal. In all these molecular liquids the hydrocarbon chains produce a WAXS scattering peak consistent with an average inter-chain distance of about 4.6 Å. Frank et al. (1993) recorded XRD patterns from n-octanol and then analyzed the SAXS patterns using a modified version of the Percus-Yevick hard-sphere theory for liquids. This theory was also tested by Chapman et al. (1990). Figure 2-5 shows the schematic drawing of the molecular organization of n-octanol. The n-octanol molecules are associated in aggregates, with their hydroxyl groups forming roughly spherical clusters and their hydrocarbon chains pointing outwards, almost fully extended (Franks et al., 1993).

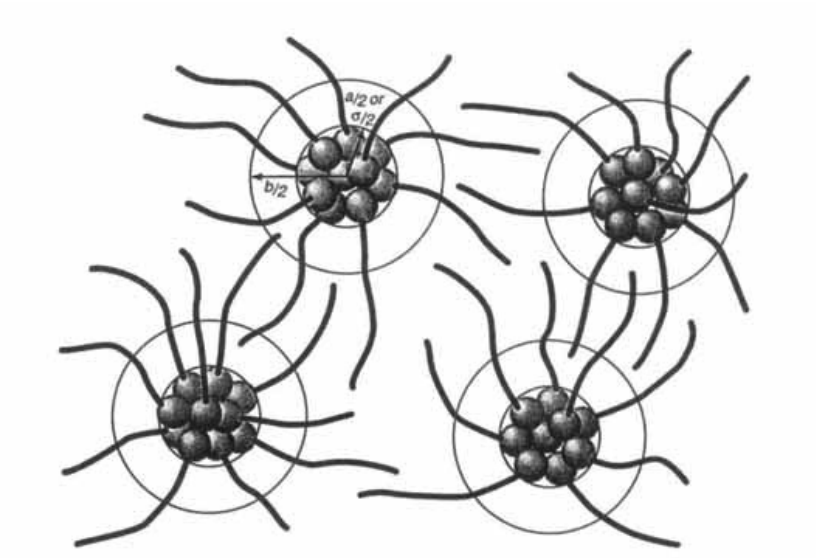

Figure 2- 5 A schematic drawing of the molecular organization of n-octanol that accounts for the observed X-ray diffraction patterns. The alcohol molecules are grouped in clusters with their hydroxyl groups approximated by either a sphere of diameter of 8.78 Å in pure n-octanol and 9.98 Å in hydrated N-octanol or a Gaussian with a FWHM of 6.22 Å in pure n-octanol and 7.08 Å in hydrated n-octanol (Franks et al., 1993).

2.2. X-ray Scattering

X-ray has long been used in studying TAGs (Clarkson & Malkin, 1948; Mazzanti et al. 2003; Metin & Hartel, 2005; Ueno et al., 1997). XRD and XRS are fundamentally similar because both methods use intense beams of X-ray to obtain structural information of the sample (Williams & Carter, 2009). Differences arise from making measurements of target molecules in solutions (XRS) or embedded in a crystal (XRD). Elastic scattering provides information on spatial distribution of electrons.

According to Bragg's law (Bragg, 1913), for a given set of lattice planes with an inter-plane distance of d (Figure 2-4), the condition for a diffraction peak to occur can be written as:

$$n\lambda = 2d \sin\theta \tag{2}$$

where λ is the wavelength of the X-ray, θ is the scattering angle and n is an integer representing the order of the diffraction peak.

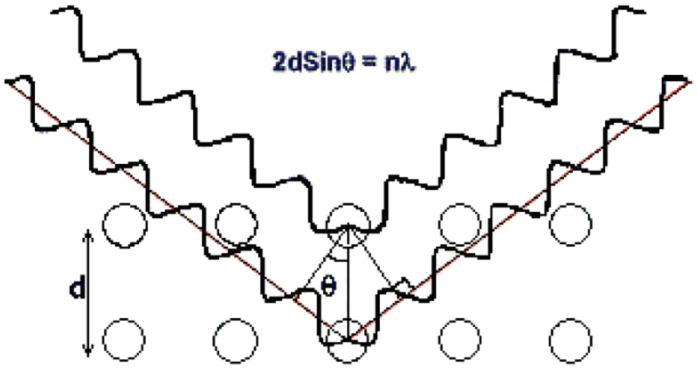

Figure 2-6 Schematic representation of X-ray scattering from a crystalline material (Bragg, 1913).

The scattering intensity is the product of the scattering amplitude by a noncrystalline array of atoms at a given reciprocal scattering vector "q" as a function of the scattering angle (Debye 1947). As presented by Klug (1974) it can be written as

$$I = \sum_m \sum_n f_m f_n \frac{\sin q \cdot r_{mn}}{q \cdot r_{mn}} \tag{3}$$

Where

$$q = (4\pi/\lambda) \sin\theta \tag{4}$$

The vector r_{mn} is an inner distance vector, pointing from the mth scattering center to the nth scattering center. The f_m are the atomic scattering densities and depend on the number of electrons of the atom and the heavier an atom the greater the f_m. Since

Bragg's law (Bragg, 1913) cannot apply strictly to XRS in liquid, Klug & Alexander (1974) came up with a general "R-spacing" corresponding to the average physical distance between scatterers:

$$R = \frac{5}{4} \times \frac{\lambda}{2 \sin \theta} = 1.25 \times d_{Bragg} \text{ with } d_{Bragg} = \frac{2\pi}{q_0} \quad (5)$$

R corresponds to a strong maximum in the diffraction pattern at angle θ and is equal to 1.25 times the *d*-spacing calculated with the aid of the Bragg equation, for a diffraction peak centered around a value of q_0 for the scattering vector. Klug however points out that the real value is likely smaller e.g. 1.22. For polymer chains, this factor was estimated to be 1.11. Klug recommended determining the value experimentally if possible.

There are two regions of XRS patterns produced by TAGs: SAXS and WAXS. WAXS shows the short distance between the aliphatic chains, and is due to the variations of electron density between atoms of neighboring molecules (or adjacent molecule branches) and the background vacuum. SAXS indicates the long distance between the glycerol cores and it is produced likely by the differences in electron density between cores and chains. Forward scattering from a single particle (Roess & Shull, 1947) is different from the inter-particle scattering (Lund & Vineyard, 1949). What we are seeing in our small angle scattering is not the forward scattering, but the inter-particle scattering. A wider angle scattering exists that is related to intramolecular electron density variations, but that is not discussed in this thesis. It corresponds to distances of less than 2 Å.

CHAPTER 3 EXPERIMENTAL METHODS AND MATERIALS

3.1. Materials

Pure LLL, MMM, PPP and SSS were chosen for this work. These TAGs are extensively distributed in nature and widely studied. Moreover, they have consecutive chain length carbon numbers (from 12 to 18), which makes easier to observe and interpret the results.

LLL, MMM, SSS and PPP samples were obtained from Sigma-Aldrich Chemical Co. with more than 99% purity and were used without further purification. Thin wall X-ray glass capillaries of 1.5 mm diameter from Charles Supper Company were used to hold the samples.

3.2. X-ray Scattering Measurements

A series of XRS experiments were performed at the beamline X10A in the National Synchrotron Light Source (NSLS, Brookhaven National Laboratory, Upton, NY, US) (Figure 3-1), and in the Dunn building of the Physics Department at Dalhousie University. Each sample was kept in a capillary at high temperature while SAXS and WAXS data were being collected.

3.2.1. Equipment

3.2.1.1. Synchrotron Radiation XRS

The beam line has energy that can be adjusted from 8 to 17 KeV. The exact energy is selected using a monochromator with two parallel crystal surfaces. A set of mirrors aligns the beam, and then it is collimated by a set of slits. The beam is further defined downstream with two more sets of slits so that when it reaches the sample it has a size of 0.5 mm x 0.5 mm. Its wavelength during our experiments was 1.0889 Å. Images of the SAXS patterns were collected to a computer by Bruker-AXS SMART software, which controls the SMART 1500 2D CCD detector camera. Meanwhile, a Laue camera manufactured by Photonic Science was used to collect the WAXS patterns. The image data were then analyzed to study the nanostructures of the liquid samples.

Figure 3-2 shows a schematic of the setup of XRS experiments performed. A temperature controller was used to monitor and control the temperature of the sample capillaries via a Labview user interface developed in our research group. WA and SA detectors were both used and a flypath full of Helium was assembled to provide a weak background. In this particular setup, both cameras were centered in a line with the flypath. Hence, the Photonic Science camera was used for capture of WAXS patterns simultaneously with SAXS patterns. The pixel size of this camera is 0.3387 mm and it was placed at a distance of 636.5 mm from the sample. The wavelength was calibrated using aluminum oxide (Al_2O_3) in a capillary and a point detector on a rotating arm centered at the crossing between the beam and the capillary. The distance was calibrated using the same capillary and capturing the WAXD pattern of the Al_2O_3 on the Laue camera. The exposure time of a WAXS pattern was set to be 4 minutes.

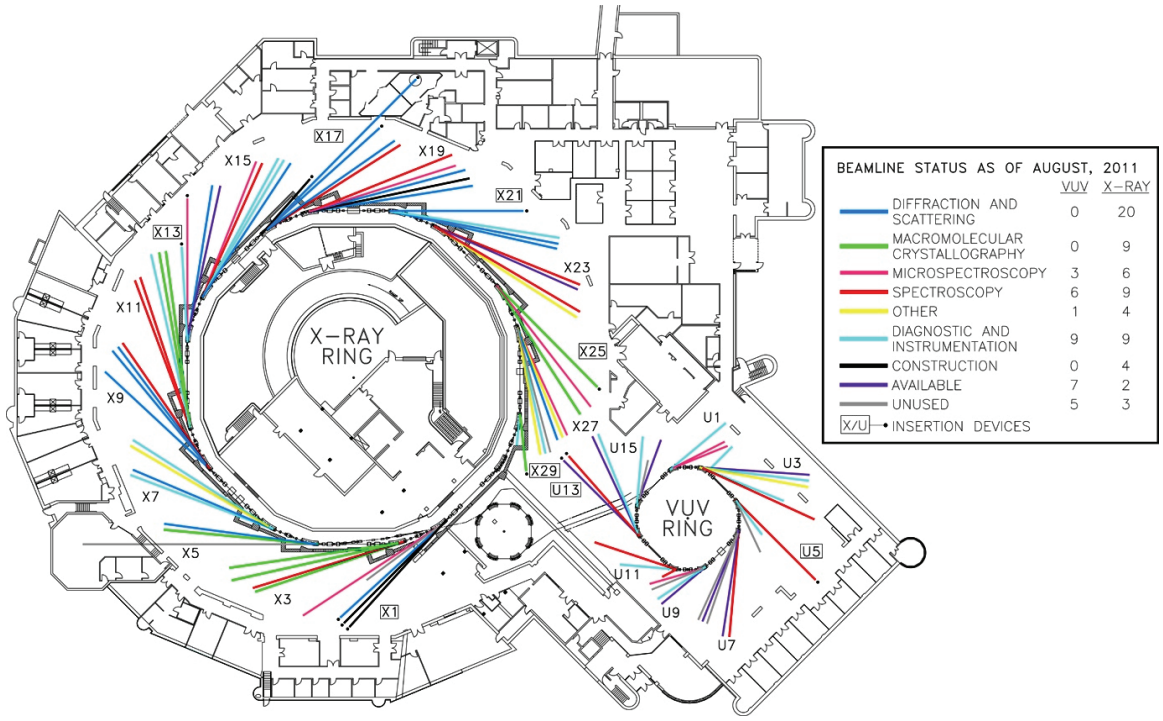

Figure 3-1 Image of the Brookhaven National Laboratory National Synchrotron Light Source (NSLS I) showing the beam line status (BNLWebsite).

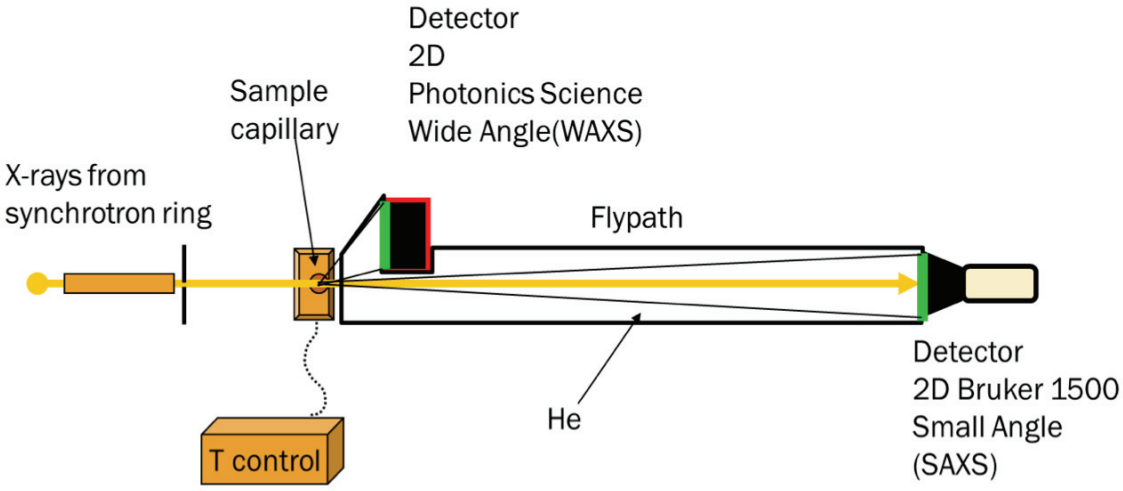

Figure 3-2 Setup of X-ray scattering experiments performed at National Synchrotron Light Source. Drawing by Dr. Gianfranco Mazzanti.

3.2.1.2. In-house XRS

The beam time in the synchrotron is limited, so in order to get more data at higher temperatures to verify our hypotheses, SAXS measurements were performed in Dr. Jeff Dahn's lab, located in the Dunn building of the Physics Department at Dalhousie University (Figure 3-3).

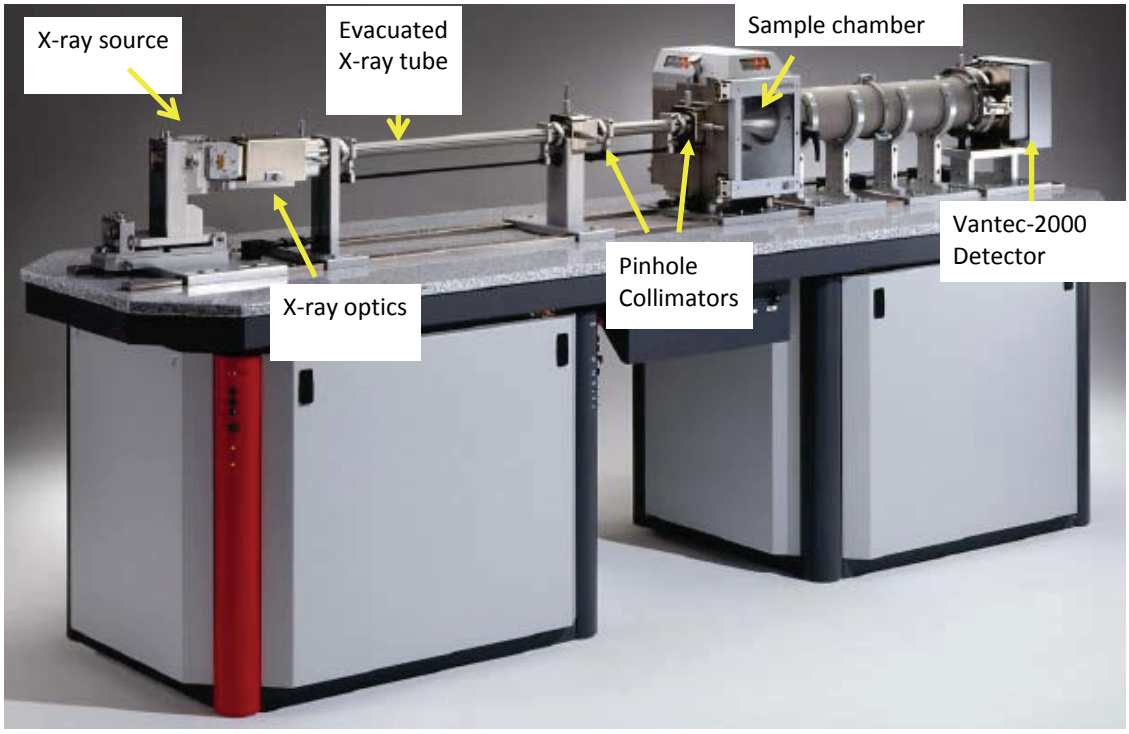

Figure 3-3 The NanoSTAR SAXS machine with components labeled. Taken from the Bruker-AXS NanoSTAR manual.

A pinhole collimated Bruker-AXS NanoSTAR equipped with a 30 W microfocus Incoatec IμSCu source and Vantec-2000 area detector was used to collect SAXS data and is shown in Figure 3-3. The generator operated at 40 kV and 650 μA, and a 400 μm diameter beam of Cu-Kα (1.541 Å) radiation was selected using pinholes and a set of

Göbel mirrors. Scattering angles ranged from 0.23 to 5.00˚. The distance from the sample to the detector was 771.78 mm calibrated with silver behenate (Ag-Beh). The exposure time of a SAXS pattern was set to be 2 hours in order to acquire satisfactory intensity. This also ensured thermal equilibrium in the capillary.

3.2.2. Sample Treatment

Liquid structure was studied at every 5°C (NSLS) and 20˚C (Dunn) within a chosen temperature range for each sample. The temperature range chosen for each sample is shown in Table 3-1 for the experiments done in the synchrotron. In the experiments done in the NSLS, five images were taken at each temperature. These temperatures were chosen based on the melting point of pure TAG samples. However, for the SAXS measurements done in the Dunn building, the equipment was left to run overnight sometimes, resulting in the unequal numbers of images at each temperature for each sample, shown in Table 3-2.

Table 3-1 Temperature profiles for X-ray scattering measurements in the NSLS beamline X10A. Temperatures are chosen at an increment of every 5°C between the temperatures.

Sample	Temperature (˚C)
LLL	40 to 95
MMM	65 to 95
PPP	60 to 105
SSS	50 to 95

Table 3-2 Numbers of images for each sample at corresponding temperatures, from the SAXS measurements in the Dunn building.

Temperature (˚C)	LLL	PPP	SSS
60	2	2	
80	2	8	3
100	8	9	1
120	1	9	6
140	10	5	3
160	1	4	2
180	5	11	8
200	8	5	3

3.3 Image Processing

X-ray scattering images were filtered using a macro developed in ImageJ to remove 'bad pixels' which were the abnormal pixels appearing in every single image due to imperfections in the detector. Then radial plots were created after the images were filtered and centered, a sample of PPP at 60˚C is shown in Figure 3-4.

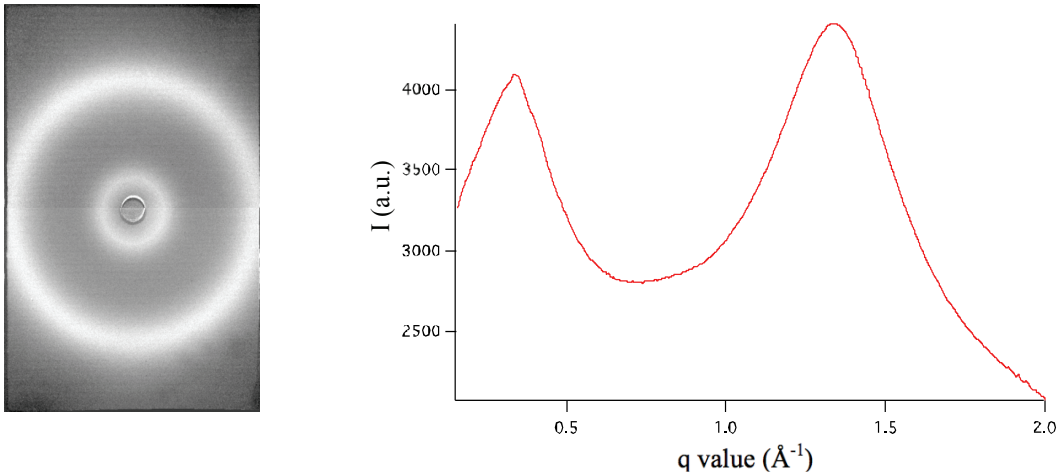

Figure 3-4 (left) An Image from Laue camera, indicating SAXS (inner circle) and WAXS (outer circle) peak. q is the scattering vector and I is the intensity of X-ray beam in arbitrary unit (a.u.). (right) Corresponding radial plot of intensity as a function of q value of PPP at 60˚C, the peak at a smaller q value is the SAXS peak and the one at a larger q value is the WAXS peak.

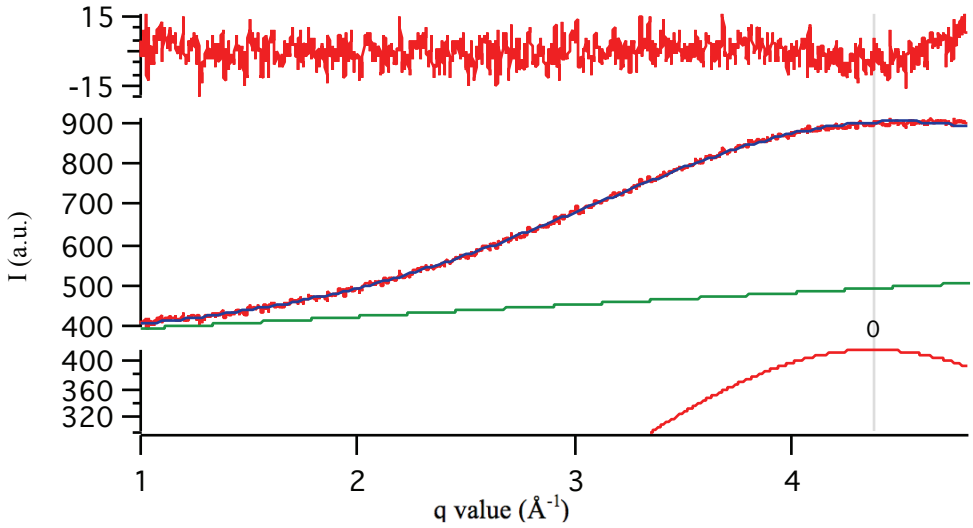

Figure 3-5 Gauss peak was fitted into radial plot of LLL at 140 ˚C from the experiment done in the Dunn building. The green line is the background, the blue line shows the experimental data, the red line is the Gauss function, and upper part shows the residuals of the curve fitting.

Then different functions were fitted into peaks using IgorPro6. Figure 3-5 shows an example of the fitted radial plot of LLL at 40 ˚C.

3.4. Electron Density Function

By means of the Fourier integral theorem, Klug (1974) simplified the scattering intensity equation and the transformation of the scattering function for identical spherical particles yields:

$$4\pi r^2\rho(r) = 4\pi r^2\rho_0 + \frac{2r}{\pi}\int_0^\infty q \cdot I(q)\sin(r \cdot q) \cdot dq \qquad (6)$$

where $\rho(r)$ is the electron density per unit volume at a distance r from the reference atom. The number of atoms contained in spherical shell of radius r is $4\pi r^2\rho(r)$, and ρ_0 is the average electron density in the sample.

Typical scattering functions are Gaussian (G) and Lorentzian (L), or a convolution

of both, i.e. Voigt. The G and L functions normalized to an area of 1 are:

$$I_G(q) = \frac{K_g}{\delta q\sqrt{2\pi}} \cdot exp\left[\frac{-1}{2} \cdot \left[\frac{K_g \cdot (q - q_0)}{\delta q}\right]^2\right] \tag{7}$$

$$I_L(q) = \frac{1}{\pi} \cdot \frac{\left(\frac{\delta q}{2}\right)}{\left(\frac{\delta q}{2}\right)^2 + (q - q_0)^2} \tag{8}$$

where the constant term K_g for the Gaussian function is:

$$K_g = 2 \cdot \sqrt{2 \cdot ln(2)} \tag{9}$$

and δq is the full width at half maximum (FWHM) of the scattered peak, q is the scattering vector and q_0 is the center value of the scattering vector of the peak. Although in a logarithmic scale the functions tend to zero in a very different way, most of the scattering information needed to characterize the structures is contained in the first two orders of magnitude of the peak. Therefore the contribution of the "tails" is of little consequence. The shape may contain some information about the structure, but it is beyond the scope of this work to interpret its meaning.

The ratio between $\rho(r)/\rho_0$ can be expressed as (Habenschuss & Narten, 1989, 1990):

$$\rho_G(r) = 1 + \frac{1}{2\pi^2 r\rho_0} \cdot \int_0^{2q_0} q \cdot I_G(q) \sin(r \cdot q)\, dq \tag{10}$$

$$\rho_L(r) = 1 + \frac{1}{2\pi^2 r\rho_0} \cdot \int_0^{2q_0} q \cdot I_L(q) \sin(r \cdot q)\, dq \tag{11}$$

From these electron density function ratios one can obtain the correction factor for R-spacing of the liquid samples for our specific experimental conditions.

CHAPTER 4 RESULTS OF THE X-RAY SCATTERING DATA

The analysis of scattering pattern images from the XRS measurements requires several steps of data reduction. These steps include filtering and unwarping the images, transferring them into data set arrays by creating the radial plots, and then fitting the scattered peaks. The fitting process provides parameters such as d-spacing values and the FWHM of the peak. The electron density ratio functions where then used to estimate the correction factor to obtain the R-spacings.

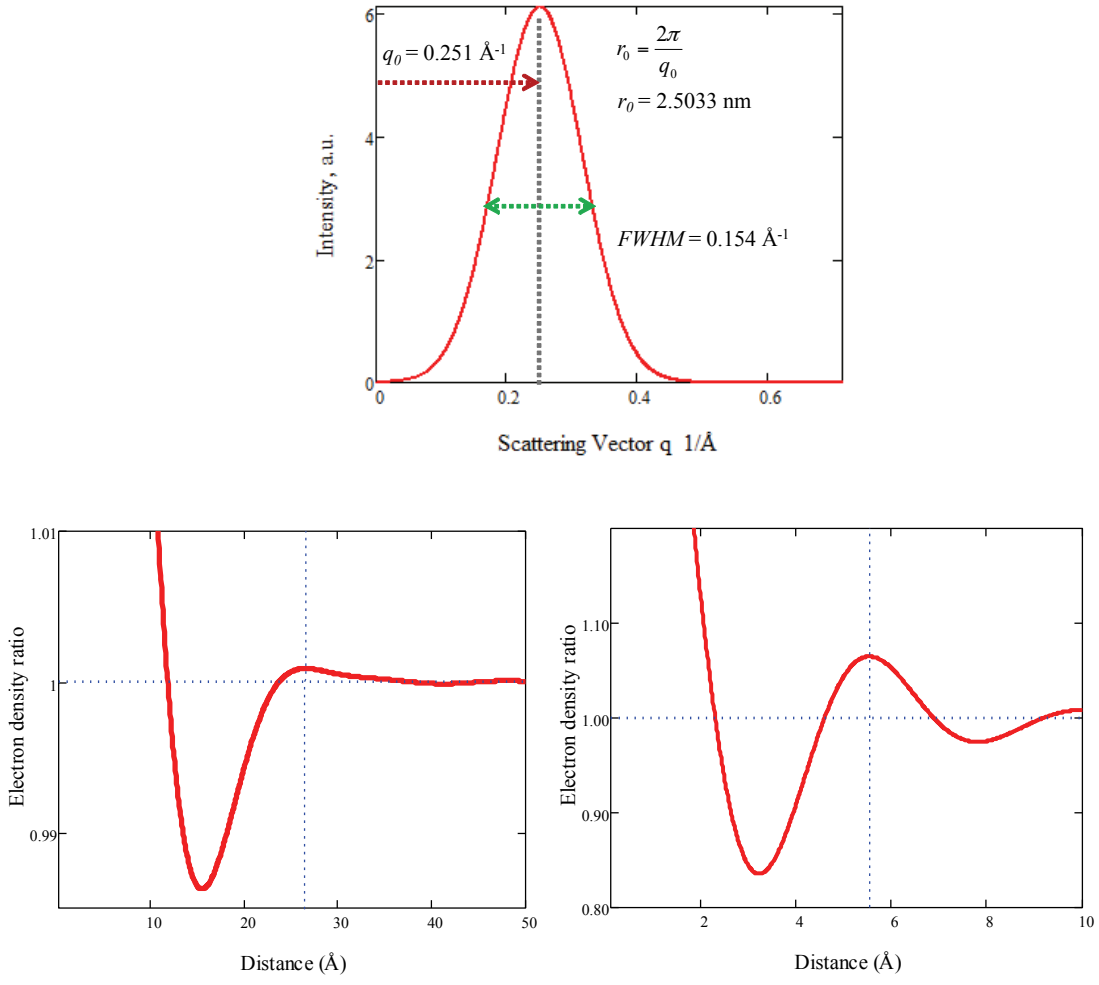

Figure 4-1 Example of electron density ratio plots. Top shows a typical small-angle liquid scattering peak. Bottom left shows a its corresponding electron density ratio plot. Bottom right shows an electron density ratio plot obtained from a typical wide angle scattering peak.

4.1. Wide-Angle X-ray Scattering Measurements

The WAXS measurements reveal short distance between atoms that either belong to different alkane chains or more frequently atoms from two different molecules (Venturi et al., 2009). Table 4-1 shows the WAXS d-spacing values of all the WAXS measurements done in the Synchrotron.

Table 4-1 WAXS d-spacing values (nm) of TAG samples from the experiment done at the NSLS beamline X10A.

Temperature (˚C)	Sample			
	LLL	MMM	PPP	SSS
40	0.4577			
45	0.4585			
50	0.4598	0.4586		
55	0.4609	0.4597		
60	0.4618	0.4607	0.4615	
65	0.4628	0.4617	0.4627	0.4620
70	0.4639	0.4627	0.4636	0.4630
75	0.4649	0.4636	0.4648	0.4641
80	0.4658	0.4647	0.4657	0.4649
85	0.4670	0.4660	0.4669	0.4661
90	0.4678	0.4667	0.4677	0.4669
95	0.4686	0.4674	0.4690	0.4678
100			0.4697	
105			0.4697	

The standard error of the d-spacing values is less than ±0.001

4.1.1. WAXS FWHM

FWHM (Table 4-2) of the liquid peaks and the type of the peaks (Table 4-3) were given by peak fitting using IgorPro.

Table 4-2 FWHM values ($Å^{-1}$) of TAG samples from the experiment done at the NSLS beamline X10A.

Temperature (˚C)	Sample			
	LLL	MMM	PPP	SSS
40	0.4423			
45	0.4457			
50	0.4509	0.3704		
55	0.4542	0.3735		
60	0.4574	0.3707	0.3534	
65	0.4603	0.3729	0.3559	0.4001
70	0.4636	0.3759	0.3565	0.4016
75	0.4665	0.3863	0.3582	0.4004
80	0.4697	0.4175	0.3585	0.4011
85	0.4733	0.4151	0.3599	0.4005
90	0.4749	0.4125	0.3614	0.3973
95	0.4776	0.4365	0.3605	0.3960
100			0.3591	
105			0.3586	

The standard error of the FWHM values is less than ±0.001.

Table 4-3 Peak type of the liquid TAG samples from the results of peak fitting in IgorPro.

Sample	WA_X10A	SA_X10A	SA_Dunn
LLL	Lorentzian	Voigt	Gauss
PPP	Voigt	Gauss	Gauss
MMM	Voigt	Gauss	Gauss
SSS	Voigt	Gauss	Gauss

4.1.2. WAXS R-spacing Values

Example calculation:

Wide-angle liquid scattering Gaussian peak (Figure 3-4) at d = 4.620 Å, which agrees with Pink et al. (2010) on the scattering peaks laid under the cluster formation, with FWHM = 1.23 $Å^{-1}$. The electron density ratio function has its first maximum at d_{max} = 5.527 Å. Ratio = 5.527/4.688 = 1.18.

The ratio was calculated for every sample at each temperature. Then we took average of the ratios and obtained $\frac{R}{d} = 1.180$, which is the correction factor for WAXS R-spacing, not too different from the value of 1.11 estimated by Klug (1974). Calculated R-spacing values are plotted against temperature in Figure 4-2.

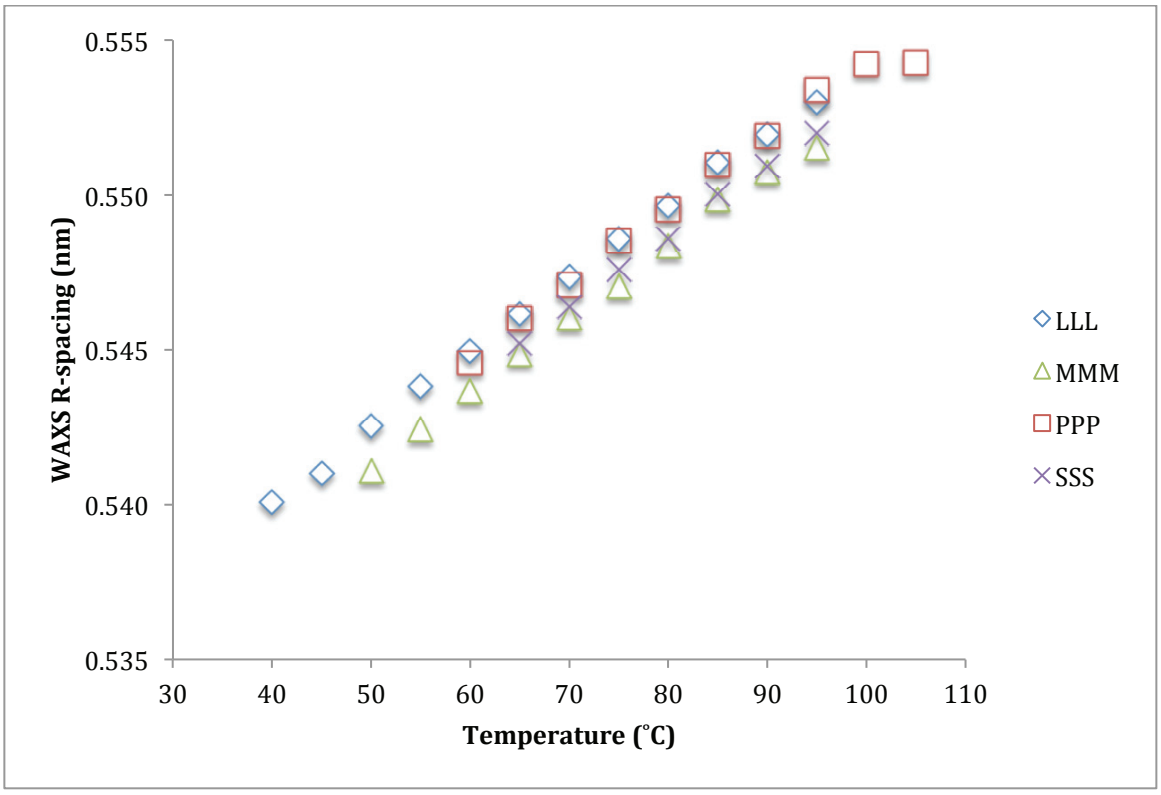

Figure 4-2 Wide-angle R-spacing values of TAG samples from the experiment done at the NSLS beamline X10A as a function of temperature.

It is clear that the R-spacing values of liquid TAGs increase almost linearly as the temperature increases, which means that the short distances between the aliphatic chains of TAGs increase with temperature. For a given Van der Waals force field, the average distances at which the attracting forces (Van der Waals) and the "repulsive forces" (thermal vibrations) equilibrate are larger at higher temperatures. Furthermore, the Van der Waals forces decrease with distance non-linearly. The linear trend in the data may be

due to the small temperature range, since the density (which changes with R^3) has been measured and is linear with temperature.

There is not much difference in R-spacing values between the samples with different carbon numbers, probably because the forces are averaged over the CH_2 groups, and hence are not very sensitive to their numbers.

4.2 Small-angle X-ray Scattering Measurements

The SAXS measurements reveal long distances between glycerol cores of TAGs. The SAXS d-spacing values of all the SAXS measurements done in the Synchrotron and the Dunn building are shown in Table 4-4 and 4-5. For the peak types, refer to Table 4-3.

Table 4-4 SAXS d-spacing values (nm) of TAG samples from the experiment done at the NSLS beamline X10A.

Temperature (˚C)	Sample			
	LLL	MMM	PPP	SSS
40	2.1090			
45	2.1004			
50	2.0861	2.3644		
55	2.0765	2.3549		
60	2.0688	2.3473	2.4478	
65	2.0604	2.3373	2.4351	2.6205
70	2.0540	2.3318	2.4259	2.6093
75	2.0484	2.3278	2.4149	2.5943
80	2.0409	2.3114	2.4081	2.5864
85	2.0347	2.2989	2.3987	2.5830
90	2.0304	2.2932	2.3927	2.5695
95	2.0252	2.2998	2.3850	2.5562
100			2.3790	
105			2.3784	

The standard error of the d-spacing values is less than ±0.01.

Table 4-5 SAXS d-spacing values (nm) of TAG samples from the experiment done in the Dunn building.

Temperature (˚C)	Sample		
	LLL	PPP	SSS
60	2.0922	2.4174	
80	2.0781	2.4022	2.5287
100	2.0578	2.3790	2.5397
120	2.0393	2.3625	2.5105
140	2.0192	2.3666	2.5084
160	2.0088	2.3569	2.5045
180	2.0023	2.3571	2.5013
200	2.0090	2.3638	2.4938

The standard error of the d-spacing values is less than ±0.01.

4.2.1. SAXS FWHM

FWHM of the liquid peaks from Synchrotron and the Dunn building are shown in Table 4-6 and 4-7.

Table 4-6 FWHM values ($Å^{-1}$) of LLL, MMM, PPP and SSS from SAXS measurements at the NSLS beamline X10A.

Temperature (˚C)	Sample			
	LLL	MMM	PPP	SSS
40	0.2165			
45	0.2113			
50	0.2071	0.1298		
55	0.2046	0.1308		
60	0.2026	0.1305	0.1225	
65	0.2005	0.1310	0.1223	0.1356
70	0.2021	0.1306	0.1220	0.1369
75	0.2019	0.1320	0.1218	0.1355
80	0.1996	0.1318	0.1212	0.1354
85	0.1967	0.1348	0.1211	0.1349
90	0.1967	0.1348	0.1203	0.1354
95	0.1972	0.1303	0.1203	0.1323
100			0.1219	
105			0.1209	

The standard error of the FWHM values is less than ±0.01.

Table 4-7 FWHM values ($Å^{-1}$) of TAG samples from the experiment done in the Dunn building.

Temperature (˚C)	Sample		
	LLL	PPP	SSS
60	0.1989	0.1470	
80	0.2069	0.1593	0.1524
100	0.2099	0.1597	0.1507
120	0.2183	0.1666	0.1671
140	0.2255	0.1661	0.1778
160	0.2327	0.1706	0.1552
180	0.2384	0.1719	0.1550
200	0.2364	0.1731	0.1518

The standard error of the FWHM values is less than ±0.01.

4.2.2. SAXS R-spacing Values

The electron density function ratio for SA R-spacing was calculated in the same way as shown for the WA, and its average value is 1.050. This value at smaller angles is not too different from 1.22 (Klug, 1974). The SA R-spacing values were calculated and plotted in Figure 4-3 and 4-4 for the synchrotron and the Dunn data, respectively.

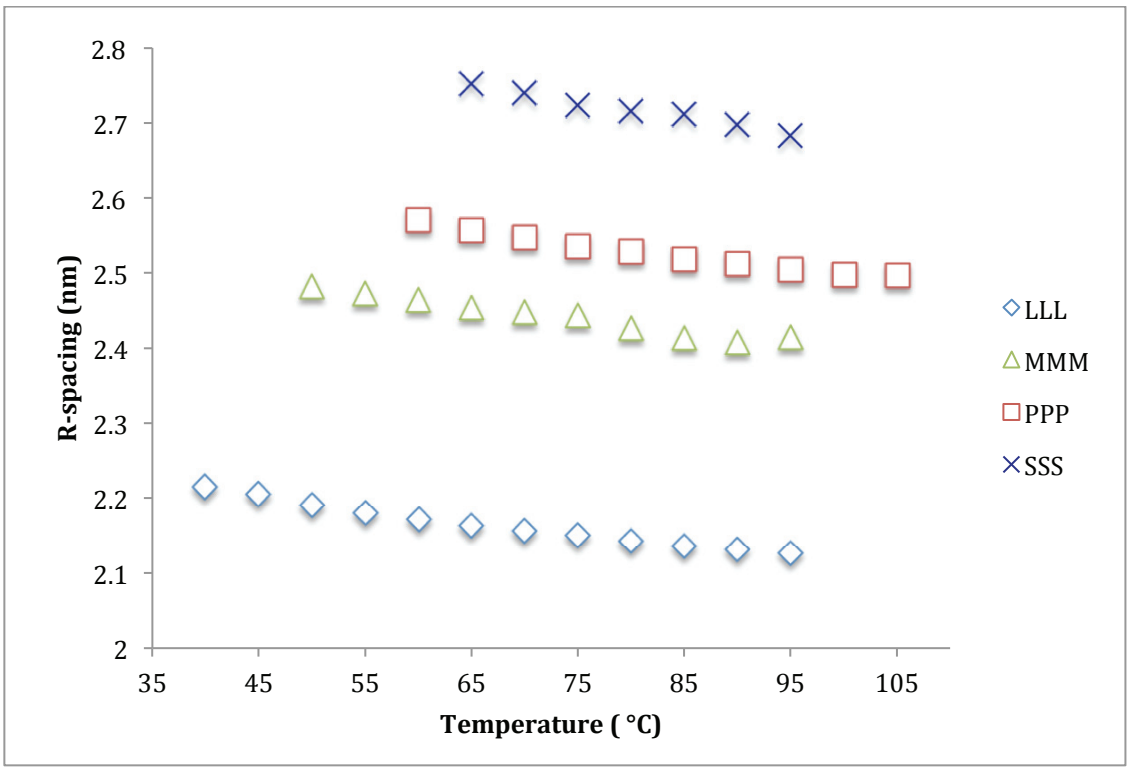

Figure 4-3 Small-angle R-spacing values of TAG samples from the experiment done in the NSLS beamline X10A as a function of temperature.

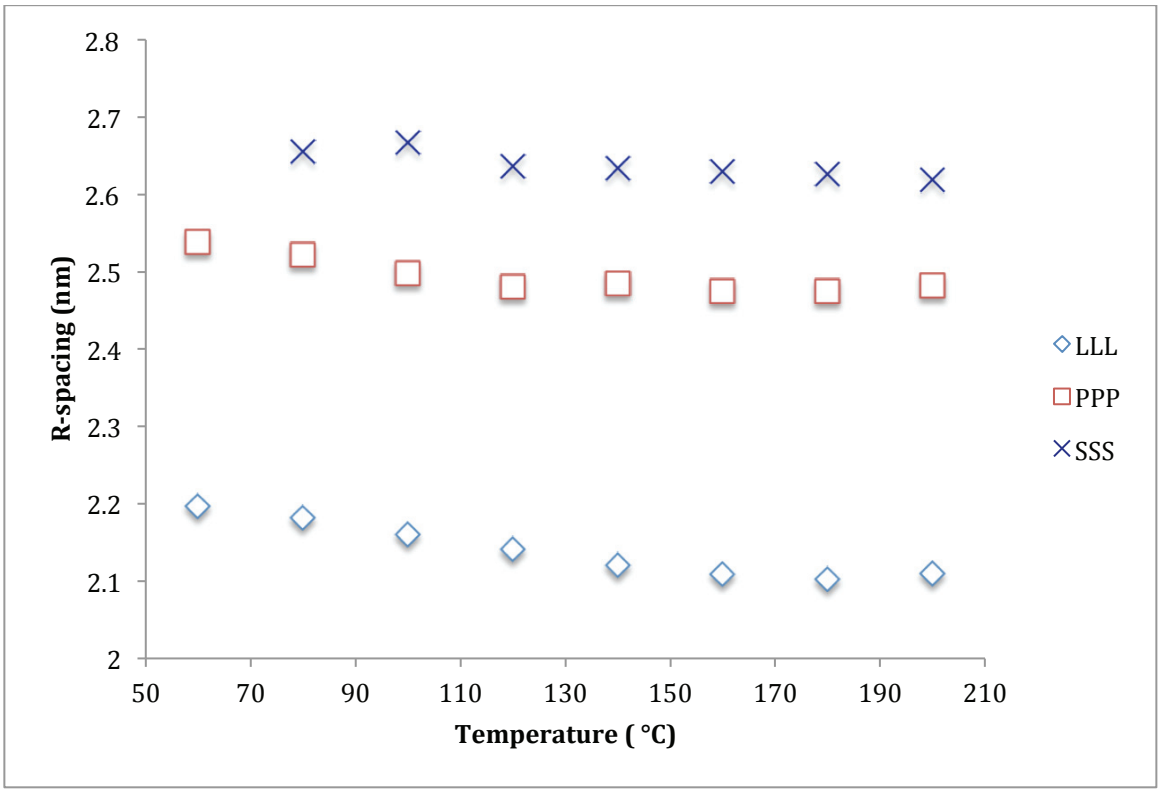

Figure 4-4 Small-angle R-spacing values of TAG samples from the experiment done in the Dunn building as a function of temperature

SAXS R-spacing values are in an inverse relation to temperature, and this means that the long distance between glycerol cores of TAGs shortens when they are heated up. With the increasing carbon number in TAGs, the R-spacing values become larger.

The SAXS R-spacing values of both measurements are not exactly the same. This is likely due to the uncertainty of the peak fitting of the SAXS data from the Dunn building. We were not able to capture the whole liquid peak (as shown in Figure 3-5) of the TAGs samples because it was difficult to adjust the distance between the sample and the detector. The SAXS R-spacing values are, however, in the same range, and the conclusions derived from both data sets turned out to be in the same range as well.

CHAPTER 5 DISCUSSION OF THE X-RAY SCATTERING DATA

The changes in liquid structures due to temperature changes should affect the R-spacing values. There are two types of molecule structures whose response to temperature is easily predictable through densities of the liquid. If the liquid structures behave as cylinder shapes, the change in R-spacing should follow equation (12a). If the structures behave as spheres, the R-spacing would follow equation (12b).

$$R_2 = R_1 \left(\frac{\rho_{m\_1}}{\rho_{m\_2}} \right)^{\left(\frac{1}{2}\right)} \tag{12a}$$

$$R_2 = R_1 \left(\frac{\rho_{m\_1}}{\rho_{m\_2}} \right)^{\left(\frac{1}{3}\right)} \tag{12b}$$

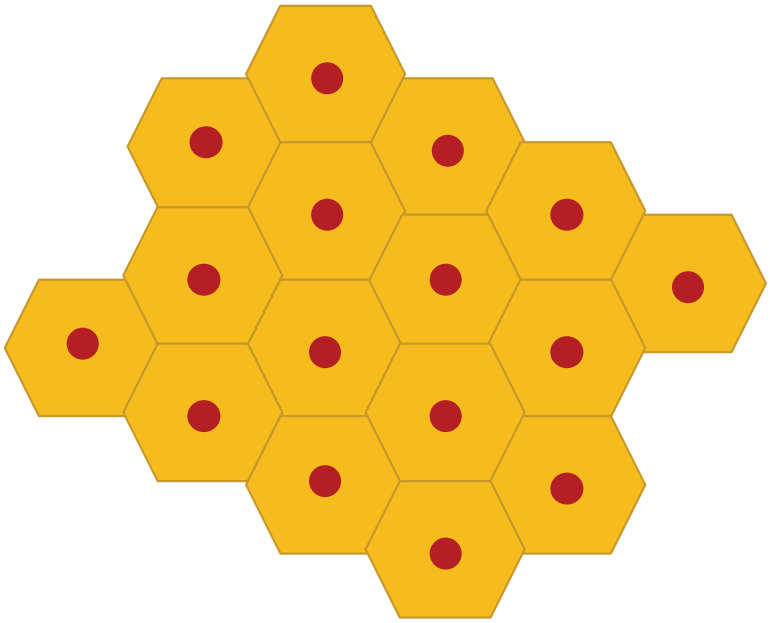

Figure 5- 1 Simple schematic of an idealized liquid made of evenly distributed space-filling molecules occupying equal volumes.

5.1 Discussion of WAXS R-spacing Values

In agreement with the cylinder structure of hydrocarbon chains suggested in the literature (Doi & Edwards, 1978a, 1978b, 1979), the average distance between primitive chains is expected to increase as the temperature increases. This happens because the volume occupied by the flexible cylinder that encloses the polymer increases. However, given this cylinder shape, the increase in cross-sectional area is proportional to R^2. Therefore, the change in distance R with T should follow equation (12a). If liquid TAGs are evenly distributed as individual molecules, and each molecule occupies equal volume (Figure 5-1), the changes in R should follow equation (12b).

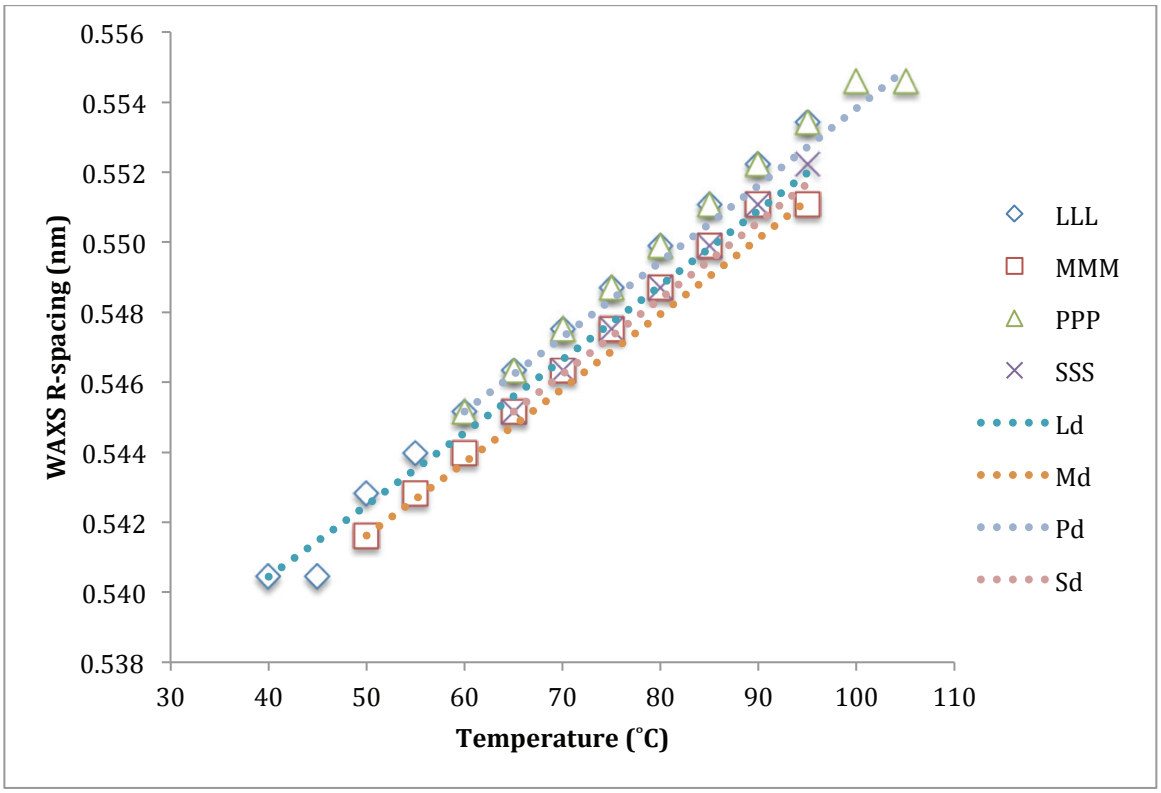

Figure 5- 2 Plots of the predicted wide-angle R-spacing value from the density of TAGs and the dotted lines are the predicted WA R-spacing values based on equation (12a), each letter corresponds to our TAG samples.

The predicted WA R-spacing values using this expression are exactly the same as the experimental ones. The simulations by Hsu & Violi (2009) indicate that there may be a recoil of up to 70% in the chains, where the average distance between the carbonyl carbon in the polar group and the last carbon of the TAG chains in the liquid is 30% less than the distance in the crystal form. This result is also consistent with the flexible cylinder concept of Doi & Edwards (1978). The aliphatic chains will thus not be fully extended radially as depicted in the concept by Franks et al. (1993) for n-octanol, but will have a higher degree of entanglement. This does not preclude that the distances between axes of the cylinders (primitive chains) depend on temperature as described above. The same situation should apply to the WA R-spacing values of unbranched alkanes (Ovchinnikov et al., 1976) with the estimated WA R-spacing values from density (Assael, Dymond, & Exadaktilou, 1994). If we were to consider that the WA R-pacing values were affected only by the "alkane behavior" of the alkyl chains, their change with temperature could be also calculated using the ratios of the densities of alkanes of the same number of carbons. It turns out that the WA R-spacing values do not follow the trend in equation (12a) when the alkanes densities are used, as shown in Figure 5-3. The interpretation of this difference is beyond the scope of this thesis.

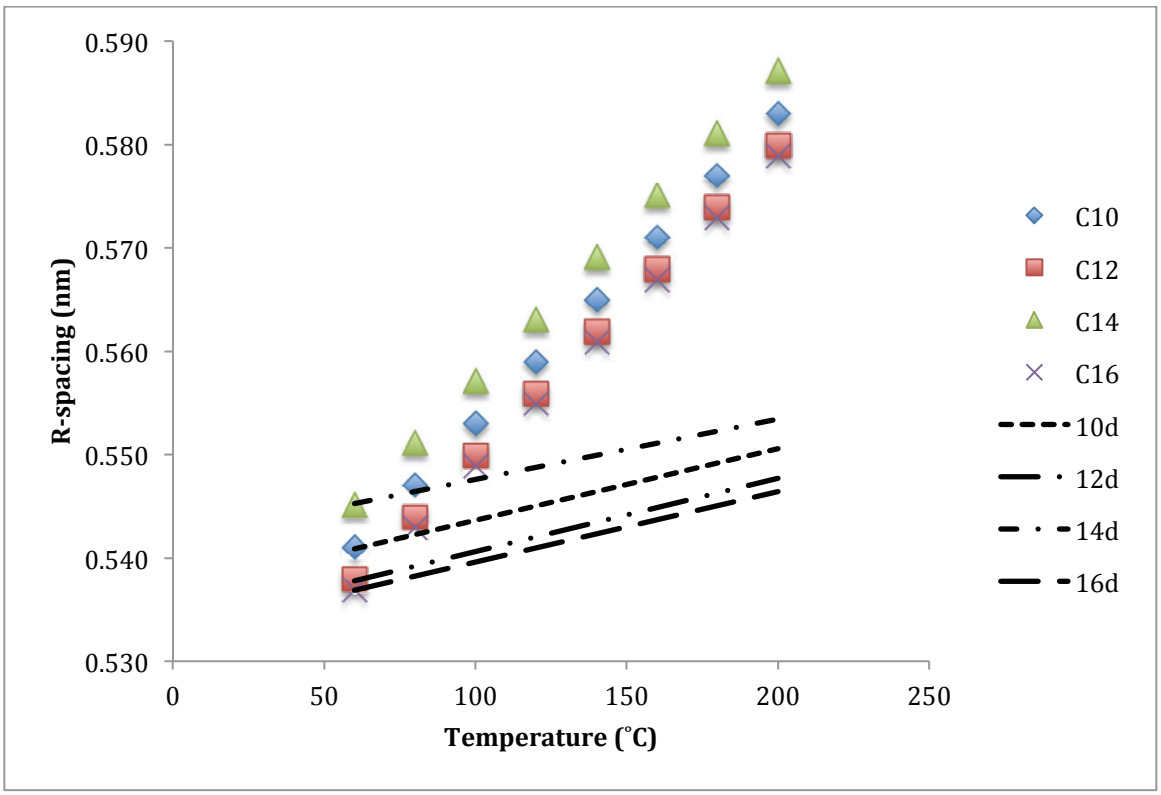

Figure 5- 3 Plots of the predicted wide-angle R-spacing values from density of alkanes with carbon numbers of 10–16, and the dotted lines are the predicted WA R-spacing values using equation 12b, each number corresponds to the carbon number of the alkane sample.

Ovchinnikov et al. (1976) investigated short-range order in liquid unbranched alkanes and polyethylene using XRS and plotted the relationship between the maximum scattering angle and the temperature, shown in Figure 5-4. Converting the scattering angle to WA R-spacing values, we compared the R-spacing values of unbranched alkanes with our TAG samples in Figure 5-5. The values of both R-spacing are in the same range.

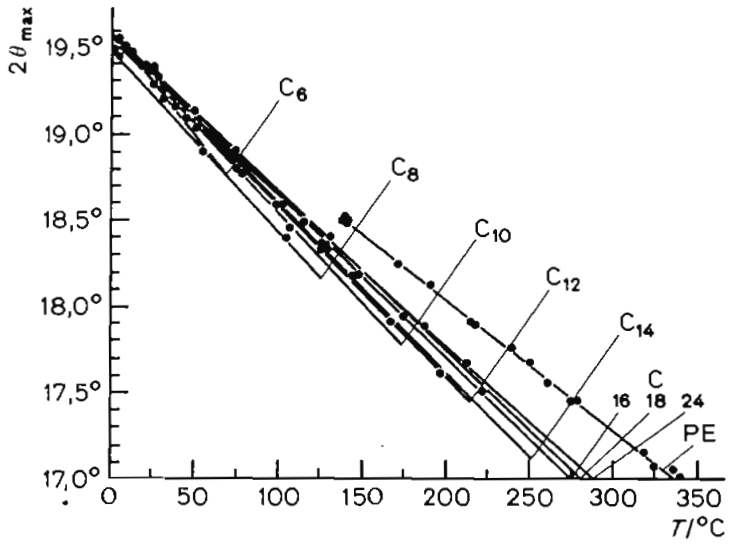

Figure 5- 4 Angle of maximum scattering $2\theta_{max}$ as a function of the temperature for unbranched alkanes C_nH_{2n+2} with even n and polyethylene (Ovchinnikov et al., 1976).

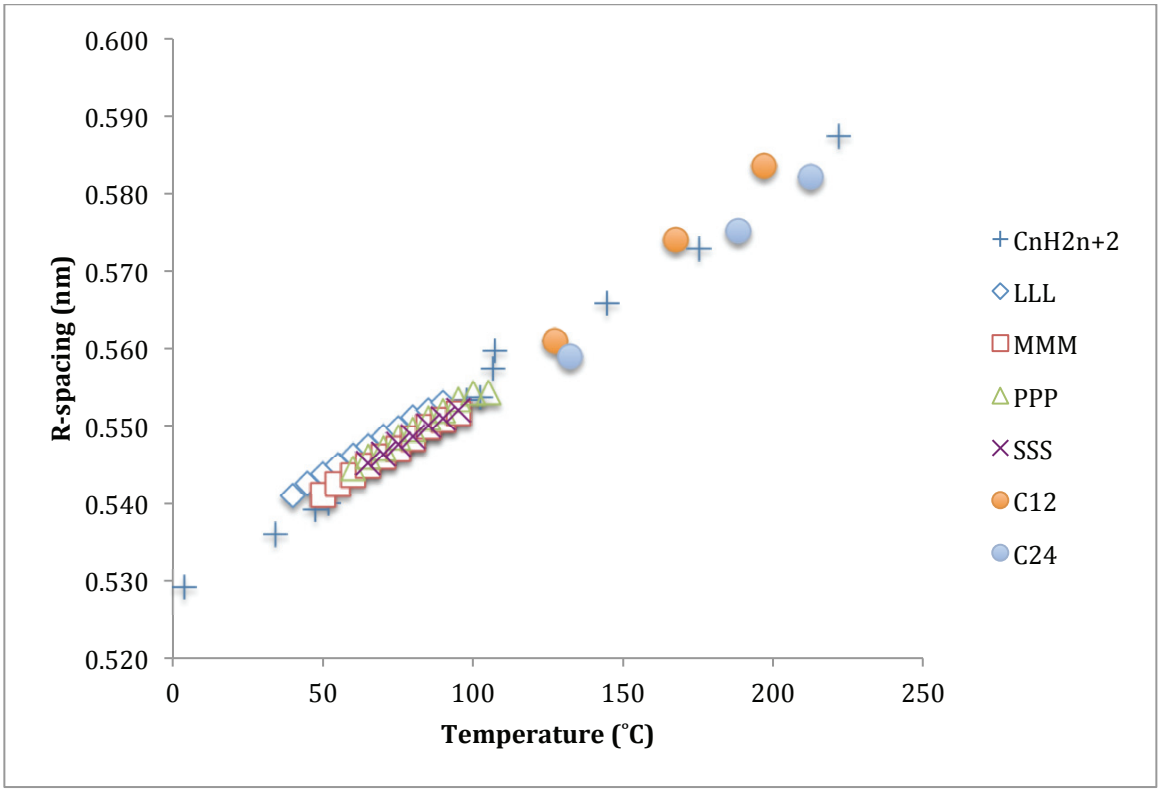

Figure 5- 5 Wide-angle R-spacing values of the unbranched alkanes (Ovchinnikov et al., 1976) compared with our TAG samples.

5.2 Discussion of SAXS R-spacing Values

Estimated from equation (12b), SA R-spacing values should follow the dotted line in Figure 5-6. It is clear that the actual SA R-spacing data we acquired from the SAXS in the Dunn building differ from the estimated values. The same applies to the data from the synchrotron.

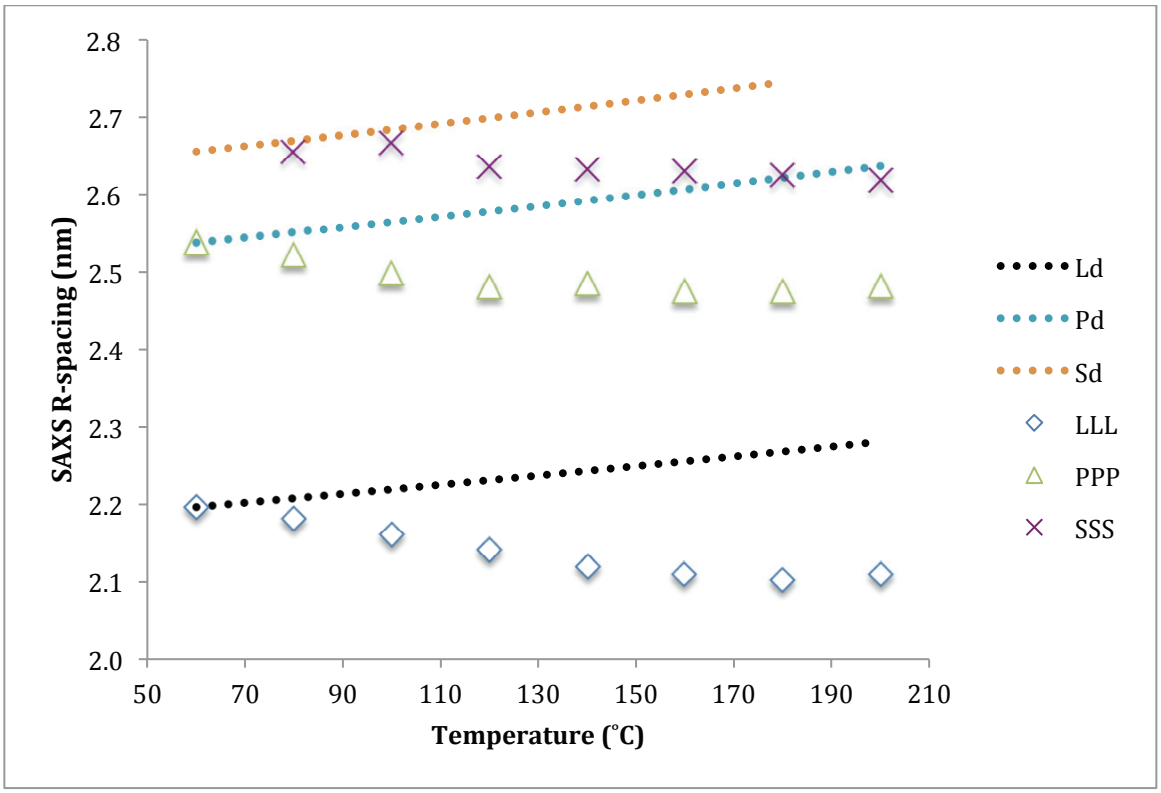

Figure 5- 6 Plots of the predicted small-angle R-spacing value from the density of TAGs and the dotted lines are the predicted SA R-spacing values using equation 12b, each letter corresponds to our TAG samples.

5.3 The Loose Multimer Model

5.3.1. Spatial Distribution of the Molecules of Liquid TAGs

The most efficient space filling packing of monodisperse (single sized) solid spheres are the hexagonal close packing arrangement (hcp) and the cubic close packing (ccp). The spheres will occupy $\pi/18^{0.5} \approx 0.74$ of the space. If the spheres are allowed to fill the rest of the space by growing equally, they will form rhombic dodecahedra (rhdh), because in the hcp, each sphere is equivalent to any other one, and each one has a coordination number of 12, i.e, touches 12 other spheres. The diameter of the sphere inscribed in the rhdh is equal to the distance between the centers of two adjacent rhdhs.

If the edge length of an rhdh is a, the radius of an inscribed sphere (r_i) is $r_i = \frac{\sqrt{6}}{3} \times a$ and the volume V is $V = \frac{16}{9} \times \sqrt{3} \times a^3$. If the volume of the space filling rhdh is known, the distance between centers (d_{c-c}) can be calculated as:

$$d_{c-c}(v) = 2 \times r_i = \sqrt[3]{\sqrt{2} \cdot v} \tag{13}$$

where v is the volume of the average rhdh that encloses the molecules.

From the Avogadro number, $N_A = 6.022 \times 10^{23}$ (molecule/mol), it is possible to determine the mass of a single molecule (M_{sm}):

$$M_{sm} = M_w / N_A \tag{14}$$

where M_w is the mass weight of TAG molecules per mole (g/mol), shown in Table 5-1.

Table 5-1 Molecular weight of TAG molecules (g/mol).

LLL	MMM	PPP	SSS
639.01	723.16	807.43	891.48

Taking PPP at 60˚C as an example, $M_{w(P)} = 807.43$ (g/mol). Then:

$$M_{sm(P)} = M_{w(P)}/N_A = 1.20\times10^{-21} \text{ (g/PPP molecule)} \quad (15)$$

Combining M_{sm} with the density (ρ), we are able to find the volume occupied by a single molecule (V_{sm}). The density depends on the composition, temperature (T), and the number of carbons in TAG molecules can characterize the composition.

5.3.2. Function to Estimate the Density of Liquid TAGs

A function to estimate the density of liquid saturated TAGs as a function of carbon number (cn) of the saturated fatty acid and temperature in °C was fitted to data from the literature (Joglekar & Watson, 1928), and the following equation was obtained:

$$\rho(cn, T) = rzk + rtk \cdot T + rck \cdot \left(\frac{18}{cn}\right)^2 \quad (16)$$

where coefficients $rzk = 903.19, rtk = -0.683$ and $rck = 14.172$. There is a good agreement between calculated and experimental values, shown in Table 5-3.

For example, the density of PPP at 60˚C is:

$$\rho_{(P)}(16{,}60) = 894.097 \ (kg/m^3) \quad (17)$$

Table 5-2 Carbon numbers of each aliphatic chain in TAG molecules.

LLL	MMM	PPP	SSS
12	14	16	18

Table 5-3 Density values (kg/m^3) for the three selected TAGs at 80 and 100 ˚C calculated using equation 15; last two columns report data available in the literature. a-(Gunstone & Padley, 1997; Kishore, Shobha, & Mattamal, 1990; Phillips & Mattamal, 1978; Rabelo, et al., 2000). b-(Sum et al., 2003).

TAG	T (˚C)	Calculated	Experiment[a]	Simulation[b]
LLL	80	880.44	882	918
	100	866.78	866	909
PPP	80	866.49	868	902
	100	852.83	854	890
SSS	80	862.72	862	895
	100	849.06	852	883

5.3.3. Prediction of Characteristic Distance Between Molecules of Liquid TAGs

If the "unit blocks" of the liquid where single TAG molecules in which the alkyl chains were crumpled around the glycerol core, we would have a simple, space filling average concept of the liquid, with individual glycerol cores separated equally (on average). To calculate the distance between these cores, we first calculate the volume of a single molecule (V_{sm}), in nm^3, by:

$$V_{sm}(cn,T) = \frac{M_{sm}}{\rho(cn,T)\cdot 1000}\cdot 10^{27} \tag{18}$$

For PPP at 60 °C:

$$V_{sm_{(P)}}(16{,}60) = 1.500\ (nm^3) \tag{19}$$

Assuming that the averaged distribution is space filling, the average characteristic distance between centers ($r_{c\text{-}c}$) in nm is:

$$r_{c-c}(cn,T) = d_{c-c}(V_{sm}(cn,T)) \tag{20}$$

and, again for PPP at 60 °C this distance would be:

$$r_{c-c_{(P)}}(16,60) = 1.285\ (nm) \tag{21}$$

which is much less than the typical experimental R-spacing value 2.448 nm.

It is thus evident from the experimental results that the molecules of the TAGs cannot be individually dispersed in their liquid state. It follows then that they must form some kind of clusters where several glycerol cores are very close, surrounded by their alkyl chains.

5.3.4. Loose Multimer Model Calculations

This solution to the centre-to-centre distance discrepancy is based on the often-remarked difference in polarity between the glycerol core of the TAGs and their aliphatic chains. The oxygen atoms at the core are permanent dipoles, especially the one with the double bond, and therefore they make this part of the molecule hydrophilic. The aliphatic chains, on the other hand, only have very weak dipoles, and are therefore hydrophobic. It has been postulated in previous research that the hydrophilic cores have stronger attraction forces between them than the aliphatic chains (Iwahashi & Kasahara, 2001). Thus some degree of association between these cores is not unlikely. In fact, many simulations show that this association is likely the case (Sum et al., 2003; Pink et al., 2010), though these simulations did not calculate the statistics of the associations. It is clear that this association determines very strongly the formation of crystalline phases. Two main defined types of associative behaviour have been previously postulated in the literature: lamellar (Larsson, 1992) and discotic (Corkery et al., 2007). We propose an alternative association, that we call the Loose Multimer model. This model is consistent with SAXS and WAXS data, and also seems to explain satisfactorily many observed properties of liquid TAGs as well as some peculiarities of their crystallization behaviour. It is also qualitatively consistent with the results of the simulations (Sum et al., 2003;

Pink et al., 2010). Since the scattering has to be produced by space zones (volumes) of different electronic density, it is reasonable to think that the hydrophilic cores have different scattering density than the space occupied by the hydrophobic chains, which are essentially an aliphatic "sea". With this in mind, we can extend the concept of the rhdh so that more than one molecule is in each rhdh, but arranged in such way that the cores are very close together, with the folded aliphatic chains wrapped around them. We call these entities Loose Multimers (LM).

They are loose because there is no strong chemical bonding between the molecules in the unit, and molecules can be exchanged between units. It is also a flexible unit, spatially speaking. They are called multimers because they have several molecules, but the numbers are not too big, as would be the case of a polymer.

The shapes of the LM do not have to be, of course, perfectly dodecahedral, but they will be some kind of squeezed deformed spheres (Figure 5-7), that change dynamically in time. They keep, however, a space filling arrangement consistent with the measured density of the liquid.

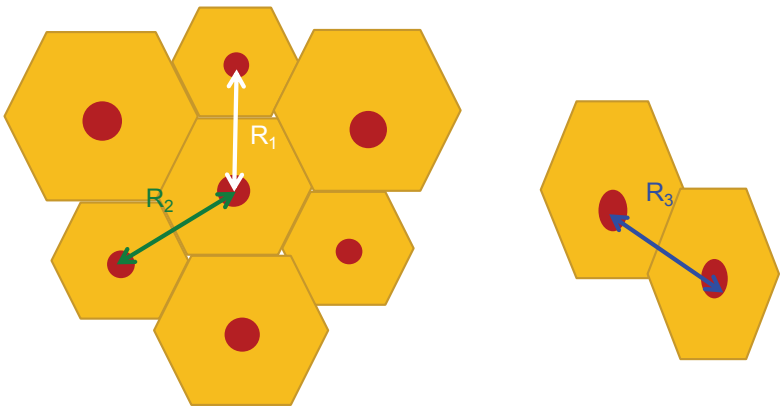

Figure 5- 7 Schematic arrangement of LM in space. R_1, R_2, R_3 represent the distance between glycerol cores of neighboring LMs.

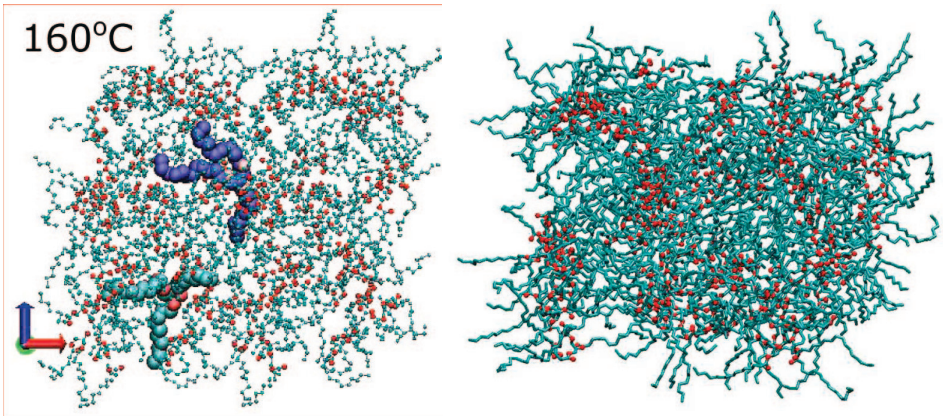

Figure 5- 8 On the left: snapshot of LLL bilayer at 160 ˚C(Hsu & Violi, 2009); on the right: snapshot of PPP at 350K at 300ns (Hall et al., 2008). The red dots represent oxygen in the glycerol cores.

In the previous studies on liquid structure of TAGs, simulations done by Hsu and Violi (2009) and Hall et al. (2008) of TAG samples in the melt show that there are aggregation of the polar groups and recoil of the aliphatic chains, as shown in Figure 5-8. Pink et al. (2010) found in simulations that di-pole forces are sufficiently large for TAG molecules to form small clusters in the melt. None of them, however, has looked into the average numbers of molecules in each cluster, which is our topic in this thesis.

For the calculation of average properties, we use the average peak position, and calculate how many molecules would there be in a LM so that both the density and the inter-center distance are satisfied. Using equation (13), and assuming an average distribution of rhdh LMs, the volume of each LM (V_{LM}) can be calculated as:

$$V_{LM}(R_{LM}) = \frac{{R_{LM}}^3}{\sqrt{2}} \tag{23}$$

where R_{LM} is the diameter of a sphere inscribed in the LM, which corresponds to the R-spacing calculated from position of the SAXS liquid peak.

For example, the volume of PPP at 60˚C is 12.006 nm^3.

By dividing the total volume of the cluster over the volume of each molecule we calculate the *average number of molecules in each LM* (N_{LM}):

$$N_{LM}(cn,T) = \frac{V_{LM}(r_{LM})}{V_{sm}(cn,T)} \tag{24}$$

and:

$$N_{LM\,(P)}(16,60) = 8.01 \tag{25}$$

5.3.5. Average number of molecules in each LM: N_{LM} Results

N_{LM} were calculated from the q_0 and R computed from the data collected for each sample at each temperature, and plotted against temperature, as shown in Figure 5-9 and 5-10. The uncertainties in the q_0 and density values are very small, but the accuracy of the R-spacing value conversion, and of the q_0 values is not well defined, though it will not change the general range of the calculated results. For instance, for PPP at 80 ˚C the average N_{LM} is 7.51 from the NSLS data, and 7.45 from the Dunn data.

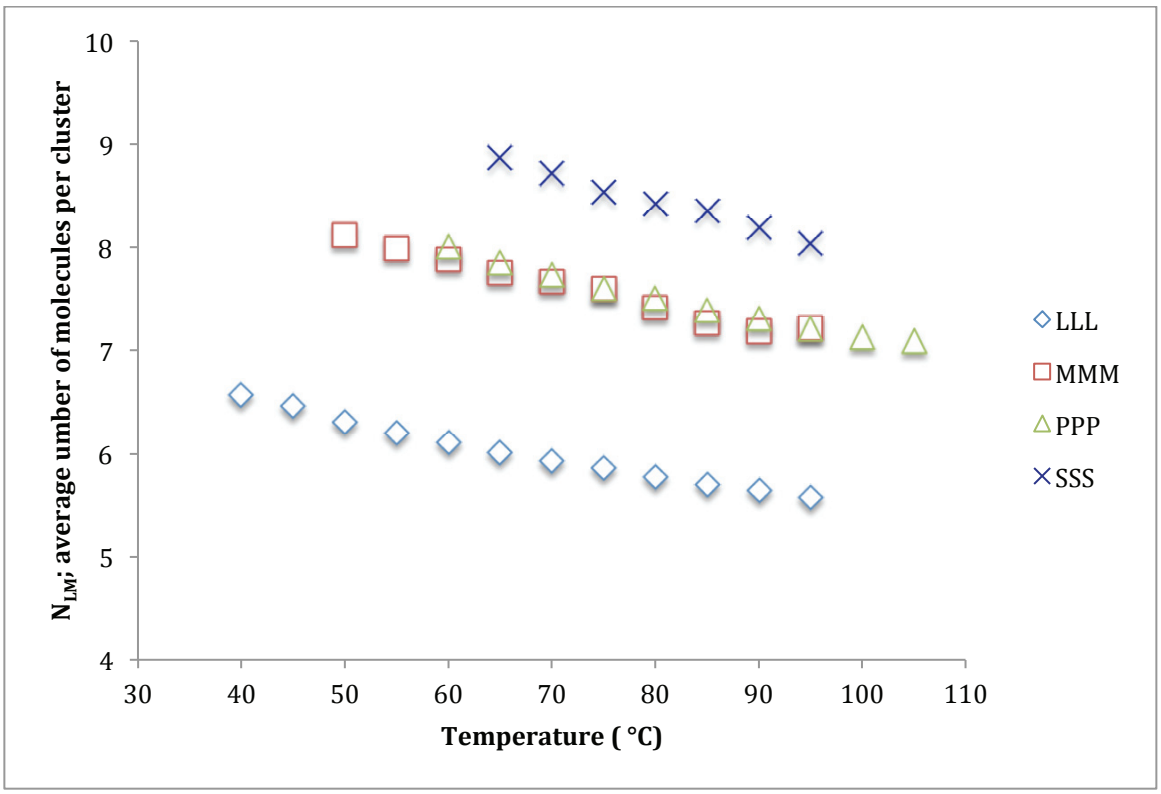

Figure 5- 9 Average N_{LM} of TAG samples from the experiment done in the NSLS beamline X10A as a function of temperature.

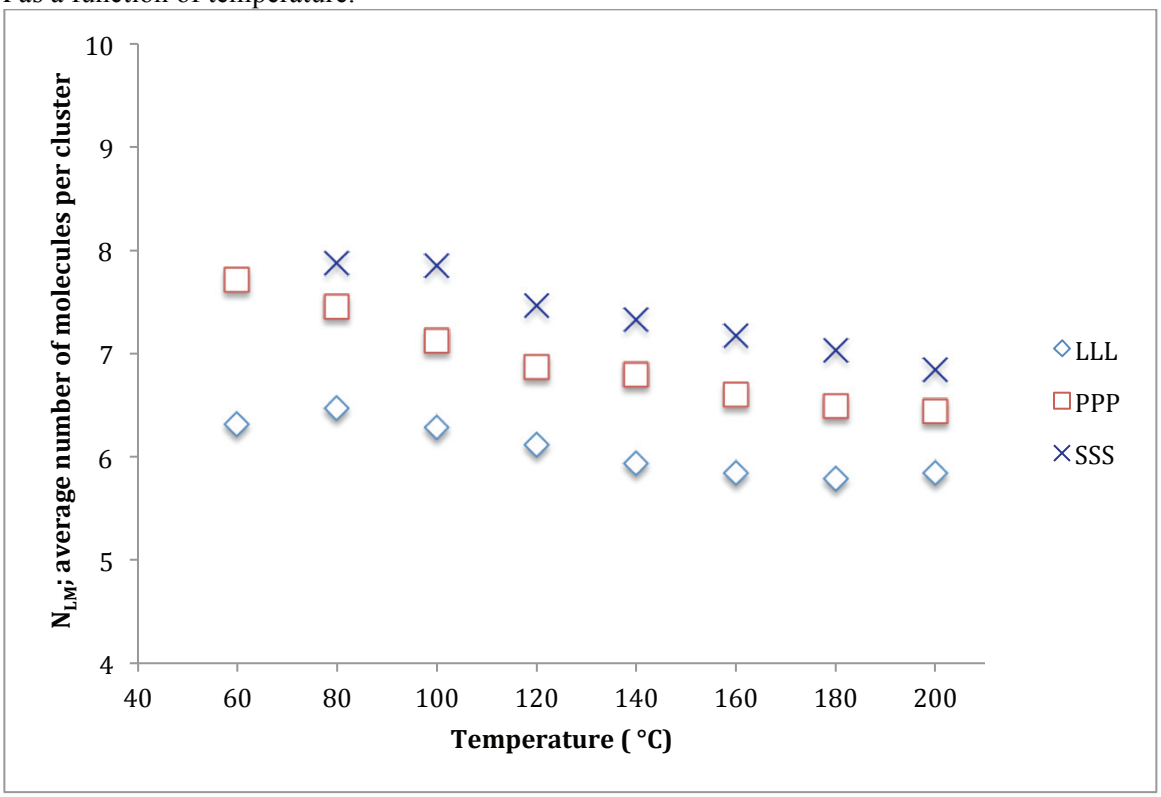

Figure 5- 10 Average N_{LM} of TAG samples from the experiment done in the Dunn building as a function of temperature.

The N_{LM} are in a range of 5 to 9. It is clearly shown in Figure 5-9 and 5-10 that with the increase of temperature, the number of molecules in each LM is reduced. The increasing temperature means that each molecule has more kinetic energy, therefore fewer molecules will stay together in a cluster, and there will be more clusters of smaller sizes. The exact distribution of cluster sizes at each temperature has not been estimated from our data, only the average value. Higher energy contents also means that a TAG molecule can move more freely from one cluster to another, and therefore the number of unattached molecules would increase with temperature. There surely is density fluctuation in the fluid at the length scale of the cluster, both inside the clusters and between clusters. However what is being observed here is the overall averaged effect of those fluctuations in both time and space. Therefore, N_{LM} represents the average number of molecules per cluster, not the exact number in every entity. The reduction of N_{LM} with increasing temperature provides a very consistent explanation for the counter-intuitive reduction of the SA R-spacing values with increasing temperature. When the temperature is increased, more clusters of smaller sizes are formed, resulting in shorter distances between the glycerol cores of TAGs.

The clustering explains why it is so difficult to form a glass, given that the clusters provide a lowered Gibbs energy barrier for crystallization nucleation to occur. This, however, does not explain so easily why these materials require such degree of undercooling before they start to crystallize. In our PPP experiments, for instance, the liquid persisted easily at 60˚C, 7.4˚C below the T_m of β PPP. On the other hand, this indicates that the energy barrier for the glass transition is higher than that for the crystallization process. This experimental observation is in agreement with the

experimental and simulation results of Pink et al. (2010), who reported that there is a discontinuous phase transition that possesses a broad metastable region. The explanation for this provided by Pink et al. (2010): even though the molecules may be clustered around glycerol groups, the methylene groups of the alkyl chains have random rotations (*trans*-*gauche*) and it takes considerable time for them to align in the all-*trans* configuration needed for crystallization.

CHAPTER 6 SUMMARY AND CONCLUSION

The goal of this work was to discover and model the distribution of TAG molecules in their liquid state, and more specifically to estimate the average number of molecules that would be found in clusters. Four pure liquid TAG samples were kept at high temperatures and examined with XRS.

The TAG molecules should fill the space of the liquid in such way that the average density of the smaller entities is equal to the density of the bulk fluid, be these entities molecules or groups of attached molecules. The simplest space filling packing of monodisperse (single sized) solid spheres are the hexagonal close packing arrangement and the cubic close packing, but the actual space filling solids are the rhdh that circumscribe the spheres. If we assume that the TAG molecules are distributed individually in the liquid, the characteristic average distance between each pair of molecules would be much smaller than the actual distance we measured from SAXS. Therefore, based on the clustering suggested by Pink et al. (2010), we developed a "Loose Multimer" model to estimate the average spatial distribution of molecules. We assume that the liquid TAGs are clustered together and arranged in such way that the cores are very close together, wrapped in the folded aliphatic chains. We call these entities "Loose Multimers". The average volume occupied by a cluster corresponds then to that of a rhombic dodecahedron. They are loose because there is no strong chemical bonding between the molecules in the unit, and molecules can be exchanged between units. Spatially speaking, it is also a flexible unit. It might not be strictly as rhombic dodecahedron, in extreme cases, the TAG molecules might lie as cylinders and cluster in

layers forming cross-like shapes. However, the forces between molecules and the exact shape still needs further discussion and advanced simulations.

By dividing the total volume of the cluster over the volume of each molecule, the numbers of molecules per cluster were calculated. These are scatterers distributed spatially that are consistent with clustering of molecules in loose multimers of 5 to 9 molecules.

The number of molecules per multimer is reduced as temperature increases, and are increased as carbon number in TAG is increased. This is the behavior expected in a fluid made of 'sticky' entities.

From WAXS, the aliphatic chains were found to behave very similarly to those of other alkyl compounds, e.g. like long flexible cylinders.

Nuclear Magnetic Resonance (NMR) experiments done by Maclean (2008) with pure and mixture samples of LLL and MMM show that there are two different diffusing species in liquid TAGs, one is fast and the other is slow. The estimated radius sizes of the slow diffusing species of LLL and MMM are around 1 nm, so the dameter would be 2 nm, which is very close to the R-spacing values obtained from our SAXS measurements. Therefore, the slow diffusing species are likely representative of clusters, while the fast diffusing species correspond probably to intra-cluster movement of the hydrocarbon chains of TAGs. The results agree generally with our model and provide a future work possibility.

This thesis sets the stage for understanding a crystallization process at the nano-level that is different from that of a homogeneous liquid. The clustering should produce a deviation in the temperature dependency of the viscosity liquid and the diffusivity of the molecules, when compared to a single molecule fluid. This may be very difficult to verify

experimentally, unless the time of formation of stable clusters is much longer than the time needed to change the temperature and perform measurements.

REFERENCES

Assael, M., Dymond, J., & Exadaktilou, D. (1994). An improved representation forn-alkane liquid densities. *International Journal of Thermophyscis*, *15*(1). Retrieved from http://link.springer.com/article/10.1007/BF01439252

Bragg, W. L. (1913). The Structure of Some Crystals as Indicated by Their Diffraction of X-rays. *Proceedings of the Royal Society A: Mathematical, Physical and Engineering Sciences*, *89*(610), 248–277. doi:10.1098/rspa.1913.0083

Callaghan, P. T., & Jolley, K. W. (1977). An irreversible liquid–liquid phase transition in tristearin. *The Journal of Chemical Physics*, *67*(10), 4773. doi:10.1063/1.434607

Cebula, D., McClements, D., Povey, M., & Smith, P. (1992). Neutron Diffraction Studies of Liquid and Crystalline Trilaurin. *Journal of the American Oil Chemist Scoiety*, *69*(2), 130–136. Retrieved from http://link.springer.com/article/10.1007/BF02540562

Chapman, W., Gubbins, K., Jackson, G., & Radosa, M. (1990). New reference equation of state for associating liquids. *Industrial & Engineering Chemistry Research*, *29*, 1709–1721. Retrieved from http://pubs.acs.org/doi/abs/10.1021/ie00104a021

Christenson, H. K., Gruen, D. W. R., Horn, R. G., & Israelachvili, J. N. (1987). Structuring in liquid alkanes between solid surfaces: Force measurements and mean-field theory. *The Journal of Chemical Physics*, *87*(3), 1834. doi:10.1063/1.453196

Clarkson, C. E., & Malkin, T. (1948). An X-ray and thermal examination of the glycerides. Part IX. The polymorphism of simple triglycerides. *Journal of the Chemical Society (Resumed)*, 985. doi:10.1039/jr9480000985

Corkery, R. W., Rousseau, D., Smith, P., Pink, D. A., & Hanna, C. B. (2007). A case for discotic liquid crystals in molten triglycerides. *Langmuir : The ACS Journal of Surfaces and Colloids*, *23*(13), 7241–6. doi:10.1021/la0634140

Da Silva, E., & Rousseau, D. (2008). Molecular order and thermodynamics of the solid-liquid transition in triglycerides via Raman spectroscopy. *Physical Chemistry Chemical Physics : PCCP*, *10*(31), 4606–4613. doi:10.1039/b717412h

De Gennes, P. (1971). Reptation of a Polymer Chain in the Presence of Fixed Obstacles. *The Journal of Chemical Physics*, *572*(1971). doi:10.1063/1.1675789

Debye, P. (1947). Molecular-weight Determination by Light Scattering. *The Journal of Physical Chemistry*, *18*(8), 18–32. Retrieved from http://pubs.acs.org/doi/abs/10.1021/j150451a002

Doi, M. (1975). An estimation of the tube radius in the entanglement effect of concentrated polymer solutions. *Journal of Physics A: Mathematical and General*, *8*(6), 959–965. doi:10.1088/0305-4470/8/6/014

Doi, M., & Edwards, S. (1978a). Dynamic of Concentrated Polymer Systems Part 3.-The Constitutive Equation. *Journal of the Chemical Society, Faraday Transactions 2*, *74*, 1818–1832. doi:10.1039/f29787401818

Doi, M., & Edwards, S. (1978b). Dynamics of Concentrated Polymer Systems Part 1.-Brownian Motion in the Equilibrium State. *Journal of the Chemical Society, Faraday Transactions 2*, 1789–1801. Retrieved from http://pubs.rsc.org/en/content/articlehtml/1978/f2/f29787401789

Doi, M., & Edwards, S. (1979). Dynamics of Concentrated Polymer Systems Part 4.-Rheological Properties. *Journal of the Chemical Society, Faraday Transactions 2*, 38–54. Retrieved from http://pubs.rsc.org/en/content/articlehtml/1979/f2/f29797500038

Franks, N., Abraham, M., & Lieb, W. (1993). Molecular Organization of Liquid n-Octanol: An X-ray Diffraction Analysis. *Journal of Pharmaceutical …*, *82*(5), 466–470. Retrieved from http://onlinelibrary.wiley.com/doi/10.1002/jps.2600820507/abstract

Fujiwara, S., & Sato, T. (1999). Molecular dynamics simulation of structure formation of short chain molecules. *The Journal of Chemical Physics*, *110*(19), 9757. doi:10.1063/1.478941

Goodsaid-Zalduondo, F., & Engelman, D. M. (1981). Conformation of liquid N-alkanes. *Biophysical Journal*, *35*(3), 587–94. doi:10.1016/S0006-3495(81)84814-X

Gunstone, F., & Padley, F. (1997). *Lipid Technologies and Applications*. CRC press. Retrieved from http://books.google.com/books?hl=en&lr=&id=MccA-I5PgIsC&oi=fnd&pg=PR9&dq=Lipid+Technologies+and+Applications&ots=LzM361KLoz&sig=o4AaUo-v9QmI8eh5sdRRxPJXiAo

Habenschuss, A., & Narten, A. H. (1989). X-ray diffraction study of liquid n-butane at 140 and 267 K. *The Journal of Chemical Physics*, *91*(7), 4299. doi:10.1063/1.456810

Habenschuss, A., & Narten, A. H. (1990). X-ray diffraction study of some liquid alkanes. *The Journal of Chemical Physics*, *92*(9), 5692. doi:10.1063/1.458500

Hall, A., Repakova, J., & Vattulainen, I. (2008). Modeling of the triglyceride-rich core in lipoprotein particles. *The Journal of Physical Chemistry. B*, *112*(44), 13772–82. doi:10.1021/jp803950w

Hernqvist, L. (1984). On the Structure of Triglycerides in the Liquid State and Fat Crystallization. *Fette, Seifen, Anstrichmittel*, *86*(8), 297–300. doi:10.1002/lipi.19840860802

Himawan, C., Starov, V. M., & Stapley, A. G. F. (2006). Thermodynamic and kinetic aspects of fat crystallization. *Advances in Colloid and Interface Science*, *122*(1-3), 3–33. doi:10.1016/j.cis.2006.06.016

Hsu, W.-D., & Violi, A. (2009). Order-disorder phase transformation of triacylglycerols: effect of the structure of the aliphatic chains. *The Journal of Physical Chemistry. B*, *113*(4), 887–93. doi:10.1021/jp806440d

Iwahashi, M., Takebayashi, S., Umehara, A., Kasahara, Y., Minami, H., Matsuzawa, H., … Takahashi, H. (2004). Dynamical dimer structure and liquid structure of fatty acids in their binary liquid mixture: dodecanoic and 3-phenylpropionic acids system. *Chemistry and Physics of Lipids*, *129*(2), 195–208. doi:10.1016/j.chemphyslip.2004.01.005

Jensen, L. H., & Mabis, A. J. (1966). Refinement of the structure of β-tricaprin. *Acta Crystallographica*, *21*(5), 770–781. doi:10.1107/S0365110X66003839

Joglekar, R., & Watson, H. (1928). The Physical Properties of Pure Triglycerides. *Journal of the Society of Chemical Industry*, *47*, 365–368. Retrieved from http://journal.iisc.ernet.in/index.php/iisc/article/viewFile/1868/1934

Kishore, K., Shobha, H. K., & Mattamal, G. J. (1990). Structural effects on the vaporization of high molecular weight esters. *The Journal of Physical Chemistry*, *94*(4), 1642–1648. doi:10.1021/j100367a077

Klug, H., & Alexander, L. (1974). *X-ray Diffraction Procedures: For Polycrystalline and Amorphous Materials, 2nd Edition*. *Willey, New York, EUA* (p. 992). Retrieved from http://scholar.google.com/scholar?hl=en&btnG=Search&q=intitle:X-ray+diffraction+procedures#2

Larsson, K. (1966). Classification of Glyceride Crystal Forms. *Acta Chemica Scandinavica*, *20*, 2255–2260.

Larsson, K. (1972). Molecular Arrangement in Glycerides. *Fette, Seifen, Anstrichmittel*, *74*(3), 136–142. doi:10.1002/lipi.19720740302

Larsson, K. (1992). On the structure of the liquid state of triglycerides. *Journal of the American Oil Chemists Society*, *69*(8), 835–836. Retrieved from http://link.springer.com/article/10.1007/BF02635928

Lund, L. H., & Vineyard, G. H. (1949). Inter-Particle Interference Effects in the Small Angle X-Ray Scattering from Fine Powders. *Journal of Applied Physics*, *20*(6), 593. doi:10.1063/1.1698433

MacLean, D. (2008). *An NMR study of diffusion in surfactant-free emulsions and molten triglyceride mixtures*. Retrieved from http://adsabs.harvard.edu/abs/2012PhDT.....432M

Mazzanti, G., Guthrie, S. E., Sirota, E. B., Marangoni, A. G., & Idziak, S. H. J. (2003). Orientation and Phase Transitions of Fat Crystals under Shear. *Crystal Growth & Design*, *3*(5), 721–725. doi:10.1021/cg034048a

Metin, S., & Hartel, R. W. (2005). Crystallization of Fats and Oils. In *Bailey's Industrial Oil and Fat Products*. John Wiley & Sons, Inc. doi:10.1002/047167849X.bio021

Ovchinnikov, Y. k., Antipov, E. M., Markova, G. S., & Bakeev, N. F. (1976). Comparative Investigation of Short-range Order in Unbranched Alkanes and Polyethylene. *Die Makromolekulare Chemie*, *177*(5), 1567–1581. doi:10.1002/macp.1976.021770524

Phillips, J. C., & Mattamal, G. J. (1978). Effect of number of carboxyl groups on liquid density of esters of alkylcarboxylic acids. *Journal of Chemical & Engineering Data*, *23*(1), 1–6. doi:10.1021/je60076a031

Pink, D. A., Hanna, C. B., Sandt, C., MacDonald, A. J., MacEachern, R., Corkery, R., & Rousseau, D. (2010). Modeling the solid-liquid phase transition in saturated triglycerides. *The Journal of Chemical Physics*, *132*(5), 054502. doi:10.1063/1.3276108

Rabelo, J., Batista, E., Cavaleri, F. vio W., & Meirelles, A. J. A. (2000). Viscosity prediction for fatty systems. *Journal of the American Oil Chemists' Society*, *77*(12), 1255–1262. doi:10.1007/s11746-000-0197-z

Roess, L. C., & Shull, C. G. (1947). XRay Scattering at Small Angles by FinelyDivided Solids. II. Exact Theory for Random Distributions of Spheroidal Particles. *Journal of Applied Physics*, *308*(1947), 308–313. doi:10.1063/1.1697651

Sato, K. (2001). Crystallization behaviour of fats and lipids — a review. *Chemical Engineering Science*, *56*(7), 2255–2265. doi:10.1016/S0009-2509(00)00458-9

Stewart, G. (1927). X-ray Diffraction in Liquids: Saturated Normal Fatty Acids, Isomers of Primary Normal Alcohols, and Normal Paraffins. *Proceedings of the National Academy of Sciences of …*, *13*(12), 787–789. Retrieved from http://www.ncbi.nlm.nih.gov/pmc/articles/PMC1085245/

Stewart, G. (1928). X-ray Diffraction in Liquid mormal Paraffins. *Physical Review*, *31*, 174–179. Retrieved from http://journals.aps.org/pr/abstract/10.1103/PhysRev.31.174

Stewart, G., & Morrow, R. (1927). X-ray Diffraction in Liquid: Primary Normal Alcohols. *Physical Review*, *30*, 232–244. Retrieved from http://journals.aps.org/pr/abstract/10.1103/PhysRev.30.232

Sum, A. K., Biddy, M. J., de Pablo, J. J., & Tupy, M. J. (2003). Predictive Molecular Model for the Thermodynamic and Transport Properties of Triacylglycerols. *The Journal of Physical Chemistry B*, *107*(51), 14443–14451. doi:10.1021/jp035906g

Takeuchi, H. (1998). Structure formation during the crystallization induction period of a short chain-molecule system: A molecular dynamics study. *The Journal of Chemical Physics*, *109*(13), 5614. doi:10.1063/1.477179

Takeuchi, M., Ueno, S., & Sato, K. (2003). Synchrotron Radiation SAXS/WAXS Study of Polymorph-Dependent Phase Behavior of Binary Mixtures of Saturated Monoacid Triacylglycerols. *Crystal Growth & Design*, *3*(3), 369–374. doi:10.1021/cg025594r

Ueno, S., Minato, A., Seto, H., Amemiya, Y., & Sato, K. (1997). Synchrotron Radiation X-ray Diffraction Study of Liquid Crystal Formation and Polymorphic Crystallization of SOS (sn-1,3-Distearoyl-2-oleoyl Glycerol). *The Journal of Physical Chemistry B*, *101*(35), 6847–6854. doi:10.1021/jp9715639

Van Malssen, K., Peschar, R., Brito C, & Schenk, H. (1996). Real-Time X-Ray Powder Diffraction Investigations on Cocoa Butter . III . Direct 13-Crystallization of Cocoa Butter : Occurrence of a Memory Effect. *Journal of the American Oil …*, *73*(10), 1225–1230. Retrieved from http://link.springer.com/article/10.1007/BF02525450

Venturi, G., Formisano, F., Cuello, G. J., Johnson, M. R., Pellegrini, E., Bafile, U., & Guarini, E. (2009). Structure of liquid n-hexane. *The Journal of Chemical Physics*, *131*(3), 034508. doi:10.1063/1.3176413

Williams, D., & Carter, C. (2009). Scattering and Diffraction. *Transmission Electron Microscopy*, 23–39. Retrieved from http://link.springer.com/chapter/10.1007/978-0-387-76501-3_2